Draft version July 30, 2025
Typeset using LaTeX **twocolumn** style in AASTeX631

Little Red Dots as self-gravitating discs accreting on supermassive stars: Spectral appearance and formation pathway of the progenitors to direct collapse black holes

Lorenz Zwick,[1] Christopher Tiede,[1] and Lucio Mayer[2]

[1]*Niels Bohr International Academy, The Niels Bohr Institute, Blegdamsvej 17, DK-2100, Copenhagen, Denmark*
[2]*Department of Astrophysics, University of Zurich, Winterthurerstrasse 190, 8057, Zurich, Switzerland*

(Dated: July 30, 2025)

ABSTRACT

We propose an alternative physical interpretation and formation pathway for the recently discovered "little red dots" (LRDs). We model LRDs as super-massive stars (SMSs) surrounded by massive self-gravitating accretion discs (SMDs) that form as a consequence of gas-rich major galaxy mergers. The model provides an excellent match for numerous spectral features of LRDs, where the V-shape arises from the superposition of two black bodies, and Balmer line broadening is sourced by the intrinsic rotation of the SMD. No additional AGN, stellar wind, dust obscuration or galactic component is required. This results in a model with uniquely few, physically motivated free parameters that are robust to variations in observed LRD properties. We perform MCMC fits for two representative LRD spectra, for which the full parameter posterior distributions are determined. Allowing for a compressed SMS mass-radius relation, the recovered parameters are compatible with sub-Eddington accretion in self-gravitating discs, and the recovered SMS masses of few 10^6 $M_\odot$ imply the subsequent formation of massive black holes (BH) that squarely follow the expected BH mass–galaxy mass relation. In addition, the model implies a redshift distribution for LRDs that accurately matches with observations.

1. INTRODUCTION

The presence of supermassive black holes (SMBHs) with masses exceeding 10^9 $M_\odot$ at redshifts $z \gtrsim 6$ presents a fundamental challenge to our understanding of structure formation in the universe (see, e.g. Bolton et al. 1963; Schmidt 1963; Zel'dovich 1964; Natarajan 2011; Volonteri 2012; Haiman 2013; Mayer & Bonoli 2019; Woods et al. 2019; Mazzucchelli et al. 2017; Lyke et al. 2020; Wang et al. 2021; Ding et al. 2022). Observed less than a billion years after the Big Bang, these objects appear far too massive to have formed naturally as a consequence of Population-III stellar evolution and the subsequent Eddington limited accretion of gas (Madau & Rees 2001; Abel et al. 2002; Schneider et al. 2002; Hirano et al. 2014).

The proposed resolutions to this enigma (excluding primordial BH scenarios, e.g. Bellomo et al. 2018; Zhou et al. 2022b,a) can be classified into two categories. The first involves invoking long periods of super-Eddington accretion, which can grow BHs from small initial masses ($\lesssim 10^3$ $M_\odot$) to the observed values at redshifts of $\gtrsim 6$. However, numerical works suggest that it is implausible to sustain such accretion rates over the required hundreds-of-millions of years due to feedback effects, black hole wandering, or a simple lack of sufficient gas supply (Alvarez et al. 2008; Smith et al. 2018; Zhu et al. 2020; Sassano et al. 2021; Fiacconi & Rossi 2016; Lupi et al. 2016; Regan et al. 2019; Sassano et al. 2022; Huško et al. 2025).

The second category involves the formation of so called "heavy seed" BHs with masses $\gtrsim 10^4$ $M_\odot$ through the direct collapse of primordial gas clouds. The most common formulation of the direct collapse scenario is via the contraction of pristine gas in dark matter halos that are illuminated by Lyman-Werner radiation from a nearby galaxy of Pop III stars (Agarwal et al. 2012; Latif et al. 2013; Regan et al. 2014; Habouzit et al. 2016; Agarwal et al. 2016; Johnson & Dijkstra 2017; Prole et al. 2024). Several complementary models aim to circumvent the need for external radiation by invoking a number of other likely relevant physics such as dynamical heating, turbulent inflow from streams, or global disc instabilities (Shlosman et al. 1989; Lodato & Natarajan 2006; Colgate et al. 2003; Koushiappas et al. 2004; Begelman et al. 2006; Begelman 2008; Latif et al. 2022). Common to these alternate formulations of direct collapse are extremely large gas inflows and the consequent formation of a highly accreting, hydrostatic spherical structure that will later undergo gravitational collapse. These structures have been modeled either as "quasi-stars" (QS) (Begelman et al. 2006; Begelman & Dexter 2025) or supermassive stars (SMS; Fowler 1966; Bisnovatyi-Kogan et al. 1967; Begelman 2010; Hosokawa et al. 2012, 2013; Haemmerlé et al. 2018a,b; Herrington et al. 2023) that culminate in sudden direct collapse due to the on-

set of catastrophic neutrino cooling or the general relativistic instability, respectively (Chandrasekhar 1964; Saijo & Hawke 2009; Begelman 2010; Shibata et al. 2016; Haemmerlé 2020) .

The recent JWST observation of a SMBH at $z \gtrsim 10$ with an estimated mass of $\sim 10^{7.6}$ $M_\odot$ (Natarajan et al. 2024; Bogdán et al. 2024) provides even greater need for the formation of intrinsically heavy black hole seeds through direct collapse. Together with other outliers (e.g. Kroupa et al. 2020; Wang et al. 2021), these systems provide strong evidence that direct collapse should occur in the early universe; and it further suggests that direct collapse models may need to produce seeds with mass $\gtrsim 10^5$ $M_\odot$.

Recently, from the observations of a novel class of JWST objects –colloquially, the "Little Red Dots"– several authors have started to suggest that we may be directly observing BH seeds, as either super-Eddington accretors (Pacucci & Narayan 2024) or as post-direct-collapse systems themselves (Naidu et al. 2025). Little red dots (LRDs) are selected by their compact (point-like) size and characteristic V-shaped spectra with red slopes in the rest-frame optical, but flat or blue colours into the UV (Matthee et al. 2024). Most LRDs present broad Balmer emission lines, suggesting that they comprise a subset of massive BHs accreting like active galactic nuclei (AGN) (Greene et al. 2024). However, producing the spectral V-shape is a challenge in standard accretion modeling, and LRDs are also almost entirely lacking in hallmark X-ray emission (Yue et al. 2024; Sacchi & Bogdan 2025). Numerous authors have also suggested that standard relations to estimate the central mass (and bolometric luminosities) from the broad lines (and optical emission) seem to break down and over-predict both quantities (Ananna et al. 2024).

In this work, we propose an alternative physical interpretation and formation pathway for LRDs. In this picture, major mergers of galaxies with $\sim 10^9$ $M_\odot$ of gas trigger strong inflows that result in a compact self-gravitating disc (SMD) at sub-pc scale, with typical temperatures of ~ 4000 K. The SMD feeds a highly accreting supermassive star (SMS) which radiates as a hot black body (~ 20000 K) due to its own accretion luminosity. We recover numerous puzzling features of LRD spectra and their cosmic abundance by allowing for a compressed SMS mass-radius relation. Crucially, the recovered parameters from spectral fitting are compatible with standard angular momentum transport mechanisms and standard Eddington limited accretion. We note that our interpretation of LRDs shares some conceptual similarities with the models recently proposed in Zhang et al. (2025)–a self-gravitating disc–and Begelman & Dexter (2025); Nandal & Loeb (2025)–a SMS-like structure. However, it differs in what parts of LRD spectra are associated to what structure and provides a unified treatment for the SMS and its accretion flow. The model does not require any additional AGN, stellar

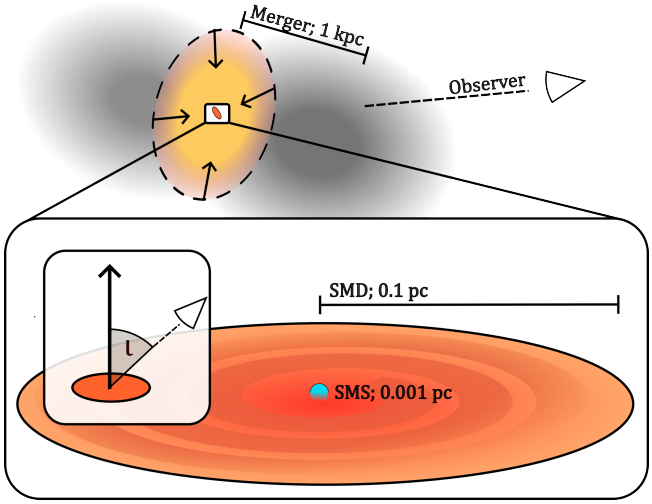

Figure 1. Simple cartoon of the assembly of a supermassive disc (SMD) and supermassive star (SMS) system that appear as little red dots (LRD). Major mergers of galaxies with at least $\sim 10^8$ $M_\odot$ of gas trigger strong inflows that result in a compact self-gravitating disc at sub-pc scale, with typical temperatures of ~ 4000 K. The disc feeds a highly accreting SMS which radiates as a hot black body (~ 20000 K) due to its own accretion luminosity.

wind, dust obscuration or galactic stellar component, resulting in few physically motivated free parameters that are robust to variations in observed LRD properties. Additionally, our model makes an explicit connection between LRDs and gas rich galaxy mergers, tying these objects with the physics of high redshift structure formation and allowing us to model the evolution of the LRD co-moving density.

The paper is structured as follows: In Sections 2, 3 and 4 we detail our model for a highly accreting SMS being fed by a SMD, noting that it naturally predicts the star and disc temperatures to match the V-shape of LRDs with very weak dependencies on physical parameters. In Section 5 we apply our model to a representative set of LRD spectra and comment on the inferred SMS and SMD properties. In Section 6 we thoroughly discuss the spectral properties of the model in the context of LRD observations, and compare the redshift distribution of observed LRDs with estimates from galaxy mergers. Finally, we present a brief summary and some concluding remarks in Section 7.

2. SMS/SMD MODEL FOR LRDS

Highly accreting SMSs in particular provide an extremely interesting precursor stage to direct collapse BHs, as they can reach masses exceeding $\sim 10^6$ $M_\odot$ before collapse. This threshold mass can be even larger if other forms of support such as rotation or magnetic fields are present (Shibata et al. 2016; Chon et al. 2018; Haemmerlé 2021; Kiyuna et al. 2024; Haemmerlé 2025). Crucially, this makes possible the creation of very massive BH seeds that retain the majority of the stellar mass (Baumgarte & Shapiro 1999; Saijo & Hawke 2009;

Reisswig et al. 2013; Woods et al. 2019, 2021) and ensures that the system can endure large accretion rates over long timescales. While SMS remain theoretical objects, both analytical studies and numerical simulations have demonstrated that a SMS-like object—accompanied by a large scale self-gravitating accretion disc—must necessarily form as a consequence of extreme gas accretion rates induced by atomic cooling halos (Regan et al. 2020; Woods et al. 2021) or the major mergers of gas rich galaxies (Mayer et al. 2010, 2015; Bonoli et al. 2014; Mayer & Bonoli 2019; Zwick et al. 2023; Mayer et al. 2024; Haemmerlé 2025). These accretion rates can be sustained down to sub-pc scales and ultimately feed a central SMS by forming a centrifugally supported disc with rotational velocities $\gtrsim 1000$ km s^{-1}, at the boundary of gravitational instability.

Our model is based on this physical picture, and is visualised in Fig. 1. The bulk of the emission consists of a superposition of two black bodies (BB) radiating according to Planck's law:

$$B_\lambda = \frac{2hc^2}{\lambda^5} \frac{1}{\exp\left(\frac{hc}{k_B T}\right) - 1} \tag{1}$$

where B_λ is the specific intensity at a wavelength λ, h is Planck's constant, k_B is Boltzmann's constant, c is the speed of light and T the BB temperature. Note that to account for redshift, the wavelengths are multiplied by the factor $\lambda_z = (1+z)\lambda_{rest}$, while the intensity is decreased by a factor $B^z_\lambda = (1+z)^{-3} B^{rest}_\lambda$. The peak wavelength of the UV component of LRD spectra is $\lambda^{peak}_{hot} \approx 0.15$ μm in the rest frame (see e.g. the spectra in Matthee et al. 2024). From Wien's Law, this corresponds to a characteristic temperature:

$$T_{hot} \sim 1.5 \times 10^4 \text{ K to } 2 \times 10^4 \text{ K}. \tag{2}$$

Similarly, the red component of the characteristic LRD spectrum often continues beyond 1 μm, implying that the colder component must have a temperature of:

$$T_{cold} \sim 2000 \text{ K to } 5000 \text{ K}. \tag{3}$$

These basic features are mentioned in several works (see e.g. Setton et al. 2024; Zhang et al. 2025; Inayoshi et al. 2025; Liu et al. 2025), noting that the LRD spectral-V is well approximated by the superposition of two blackbodies with these characteristic temperatures. Given the difference in temperature and the similarity of the flux in the hotter and the colder portions of typical LRD spectra, we can also deduce that the hot BB component must have an emitting area that is much smaller than the cold component, roughly by a factor $(T_{cold}/T_{hot})^2 \sim 100$.

In our model, the hot component consists of a highly accreting SMS with radius R_S and temperature T_S. The star is

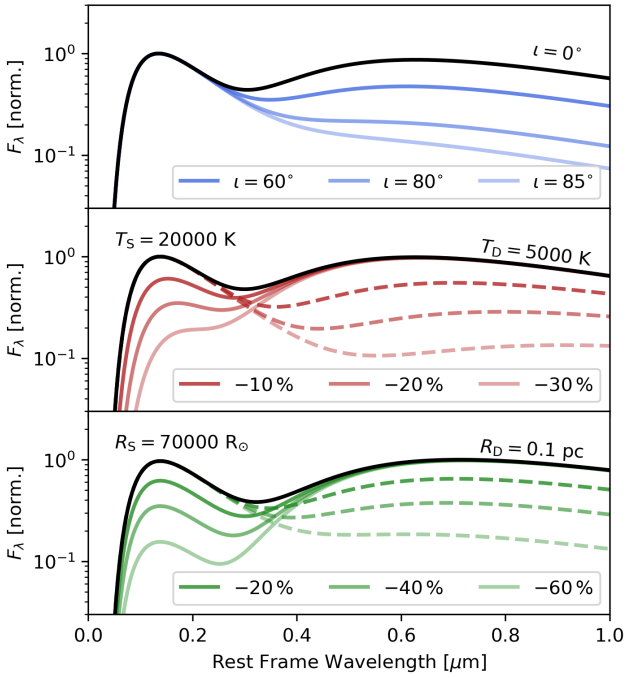

Figure 2. Basic spectra of the composite SMS/SMD model for different system inclinations (top panel), component temperatures (middle panel) and component sizes (lower panel). The chosen reference parameters are representative for the best fits of typical LRD spectra (see section 5). We highlight the different behaviours of the model by changing a single parameter at a time by the amount shown in the labels, with respect to a baseline choice represented by the black lines. In the bottom two panels, solid-lines indicate the hot SMS component and dashed-lines the cool SMD. Note that the inclination, mass and temperature of the disc become fully determined by spectral fitting once additional physical constraints are adopted (see section 5).

accreting from a surrounding, cooler accretion disc of characteristic radius R_D, temperature T_D, and scale-height H_D. The rest frame BB flux F^S_λ seen at a luminosity distance D_L from the SMS is:

$$F^S_\lambda = \pi \frac{R_S^2}{D_L^2} B_\lambda(T_S), \tag{4}$$

and does not depend on the viewing angle (valid under the assumption of a thin accretion disc, which we will discuss in more detail in sections 4 and 5). In contrast, the disc's BB flux F^D_λ depends strongly on viewing angle. We define the projection angle ι to range between 0 and $\pi/2$, where $\iota = 0$ represents a fully face on disc, while $\iota = 90°$ represents an edge on disc:

$$F^D_\lambda = \pi \frac{4\pi R_D^2 \cos(\iota) + 4 H_D R_D \sin(\iota)}{4\pi D_L^2} B_\lambda(T_D). \tag{5}$$

Lastly, the majority of LRDs present with broadened H$_\alpha$ and H$_\beta$ lines which are typically attributed to Keplerian gas

clouds rotating a central SMBH, known as broad-line regions (Antonucci 1993). In our model, the broadening of the lines is instead caused by the intrinsic rotation of the accretion disc under its own self gravity. The line-broadening velocity is then given by the disc's circular velocity:

$$v_{\rm D}^{\rm rot}\sin(\iota) \equiv \sqrt{\frac{GM_{\rm D}}{R_{\rm D}}}\sin(\iota), \tag{6}$$

where $M_{\rm D}$ is the total mass of the disc and we projected the disc's rotation along the line of sight. Reaching rotational velocities of thousands of km/s requires discs that are more massive and compact than atomic cooling halos (Prieto et al. 2013; Regan et al. 2020; Prole et al. 2024). The required typical scales are:

$$v_{\rm D}^{\rm rot} \approx 2000 \left(\frac{0.1\,{\rm pc}}{R_{\rm D}}\cdot\frac{M_{\rm D}}{10^8\,{\rm M}_\odot}\right)^{1/2} {\rm km/s}\,. \tag{7}$$

The formation of such "super massive" discs (SMDs) has been verified to occur in high-resolution numerical studies of major galaxy mergers from both individual merger simulations (Mayer et al. 2010, 2015) as well as full cosmological zoom-in simulations (Mayer et al. 2024) because of the rapid removal of gas angular momentum in shocks or from galactic tidal forcing (see also Mihos & Hernquist 1996; Lambas et al. 2012). More broadly, SMDs or similar forms of accretion flow are motivated by the immense gas requirements necessary to fuel any model of BH growth and explain the high masses of quasars. We will discuss the expected properties of SMDs in more detail in section 4.

To summarise, our model for LRDs consist of a smaller, hotter highly accreting SMS surrounded by an extended and self-gravitating SMD. Overall, the model has a small set of parameters which are listed in Table 2, and their effect on the basic spectral model is shown in Fig. 2. As we will see in the following sections, these parameters can be used in combination with several physical relations and constraints to precisely determine the SMS and SMD mass, stability, lifetime and other properties by fitting the resulting model spectra to observations of LRDs.

3. ACCRETING SUPERMASSIVE STARS

3.1. *SMS accretion and temperature*

We consider the case in which the accretion power drives the luminosity of the star. In this scenario, the kinetic energy of gas accreting onto the star is thermalised via shocks and other dissipative processes upon reaching the stellar surface (Frank et al. 2002). The typical velocity of a fluid element close to the SMS is dominated by the star's gravitational potential, and is therefore of the order of the circular velocity:

$$v_{\rm S}^{\rm c} = \sqrt{\frac{GM_{\rm S}}{R_{\rm S}}}, \tag{8}$$

$R_{\rm S}$	SMS radius
$T_{\rm S}$	SMS temperature
$f_{\rm c}$	SMS compression factor
$R_{\rm D}$	SMD radius
$T_{\rm D}$	SMD temperature
$n_{\rm D}$	SMD density
$h_{\rm D}$	SMD aspect ratio
ι	System line of sight inclination

Table 1. The SMS/SMD spectral model parameters, which are related to physical properties of SMSs and self-gravitating discs as detailed in sections 3 and 4. These are to be understood as characteristic values that describe the general features of the spectrum. The parameters are recovered by fitting a two component BB model to the observed spectra, associating the broadening of the hydrogen lines to the rotation of the SMD and enforcing several physical constraints for both the SMS and the SMD.

where $M_{\rm S}$ is the SMS mass. Therefore, the associated accretion power is:

$$P_{\rm acc} = \frac{\eta_{\rm acc}}{2}\dot{M}_{\rm S}v_{\rm c}^2, \tag{9}$$

where the efficiency of the thermalisation is described via a dimensionless parameter $\eta_{\rm acc}$, and $\dot{M}_{\rm S}$ is the accretion rate onto the SMS. To obtain a SMS temperature, we equate the accretion power to the radiated BB power $P_{\rm BB} = 4\pi R_{\rm S}^2\sigma_{\rm B}T_{\rm S}^4$ of the SMS, yielding a relation between the star's temperature, mass, radius and accretion rate:

$$T_{\rm S}^4 = \frac{\eta_{\rm acc}}{8\pi}\frac{GM_{\rm S}\dot{M}_{\rm S}}{\sigma_{\rm B}R_{\rm S}^3}. \tag{10}$$

Evaluating for some typical SMS parameters gives:

$$T_{\rm S} \approx 6.11\times10^3 \left(\eta_{\rm acc}\frac{M_{\rm S}}{10^5\,{\rm M}_\odot}\cdot\frac{\dot{M}_{\rm S}}{10^2\,{\rm M}_\odot\,{\rm yr}^{-1}}\right)^{1/4} \times\left(\frac{R_{\rm S}}{5\times10^4\,R_\odot}\right)^{-3/4}{\rm K}\,, \tag{11}$$

where we recover the often quoted effective temperature of $\sim$ 5000 K for SMSs (see e.g. Fowler 1966; Hosokawa et al. 2013). Expressing the temperature in terms of our model observables on the right hand side, we can constrain a combination of the accretion rate, stellar mass and accretion efficiency to:

$$\eta_{\rm acc}M_{\rm S}\dot{M}_{\rm S} = \frac{8\pi\sigma_{\rm B}}{G}T_{\rm S}^4R_{\rm S}^3. \tag{12}$$

The outer envelopes of SMSs are radiation pressure supported, and their evolution is bound by the Hayashi limit, which marks the onset of global convective instabilities (Hayashi 1961). Numerical simulations for accretion rates of order $\gtrsim$ 0.01 ${\rm M}_\odot$ ${\rm yr}^{-1}$ have found the radius of SMSs to

be well approximated by (Hosokawa et al. 2013):

$$R_{\rm S}^{\rm Hos} \approx 260\,{\rm R}_\odot \left(\frac{M_{\rm S}}{{\rm M}_\odot}\right)^{1/2}, \tag{13}$$

up to masses of several 10^4 $\mathrm{M}_\odot$, and this relation is often extrapolated to higher masses (see e.g. Haemmerlé et al. 2021). However, there are several arguments that suggest that more compact SMSs may exist, and may even be preferred depending on the physical properties of the system. We parametrise the uncertainty in the SMS mass radius relation phenomenologically, by introducing a compression factor $f_{\rm c} < 1$ such that $R_{\rm S} = f_c R_{\rm S}^{\rm Hos}$ and

$$\frac{M_{\rm S}}{{\rm M}_\odot} = f_{\rm c}^{-2} \left(\frac{R_{\rm S}}{260\,{\rm R}_\odot}\right)^2. \tag{14}$$

This provides an estimate of the SMS mass given a recovered value for the SMS radius from the hot BB component of our model spectrum. We discuss typical values of $f_{\rm c}$ in detail in section 3.2 and 5.2.

The SMS mass radius relation also sets a maximum allowed accretion rate onto the surface of the SMS that is consistent with purely gravitational physics. This limit has been derived in Haemmerlé et al. (2021) for non-compressed SMSs following the mass-radius relation of Eq. 13. We report it here with a simple modification to account for a possible compression:

$$\dot{M}_{\rm S}^{\rm max} \approx 2\times10^4\, f_{\rm c}^{-3/2} \left(\frac{M_{\rm S}}{10^4\,{\rm M}_\odot}\right)^{3/4} {\rm M}_\odot\,{\rm yr}^{-1}, \tag{15}$$

where the scaling of $f_{\rm c}^{-3/2}$ arises from the simple dependence of the limit with the gravitational compactness of the accretor. We parametrise the actual accretion rate on the SMS as a fraction $f_{\rm acc} < 1$ of the maximally allowed rate, i.e. $\dot{M}_{\rm S} = f_{\rm acc}\,\dot{M}_{\rm S}^{\rm max}$. Given this parametrisation, we can use the mass radius relation and the accretion rate to express the effective BB temperature of a SMS simply as a function of its mass and a few dimensionless numbers:

$$T_{\rm S}^4 = \frac{\eta_{\rm acc} f_{\rm acc} f_{\rm c}^{-9/2}}{8\pi} \frac{G M_{\rm S} (20\,{\rm M}_\odot\,{\rm yr}^{-1})}{\sigma_{\rm B} (260\,{\rm R}_\odot)^3} \left(\frac{M_{\rm S}}{M_\odot}\right)^{-3/4}. \tag{16}$$

Evaluating for some typical parameters gives:

$$T_{\rm S} \approx 2.4\times10^4\, \eta_{\rm acc}^{1/4} f_{\rm acc}^{1/4} f_{\rm c}^{-9/8} \left(\frac{M_{\rm S}}{10^5\,{\rm M}_\odot}\right)^{1/16} {\rm K}. \tag{17}$$

For efficiencies $\eta_{\rm acc} \lesssim 1$, we see that the temperature of tens of thousands of Kelvin required to explain the UV emission peak in LRD spectra is, in principle, entirely consistent with allowed accretion rates of $f_{\rm acc} < 1$, especially when considering possible compression factors $f_{\rm c} < 1$. Additionally, an important result is that this temperature scales extremely weakly with mass, such that variations in system specifics would not influence the general appearance of SMSs. This suggests that SMSs provide a consistent and robust explanation for the characteristic UV emission from LRDs.

Finally, we note that during the SMS phase extremely high accretion rates can be sustained without violating the Eddington limit (even though super-Eddington accretion is commonly invoked to explain LRDs). Setting the accretion luminosity equal to the Eddington luminosity (Eddington 1921) we find:

$$\dot{M}_{\rm S}^{\rm Edd} = \frac{8\pi c}{\eta_{\rm acc}\sigma_{\rm T}} R_{\rm S} \approx 104.5 \left(\frac{R_{\rm S}}{5\times10^4\,{\rm R}_\odot}\right) {\rm M}_\odot\,{\rm yr}^{-1}. \tag{18}$$

While we do not enforce sub-Eddington accretion explicitly in our model fitting, we will use Eq. 18 to discuss the possible estimates for the compression factor $f_{\rm c}$ in section 5. We will, in fact, find solutions that do not require exceeding this limit.

3.2. *Constraints from SMS relations*

Collecting Eqs 11 and 15 we find that a measurement of SMS temperature and SMS radius from the spectral model ($T_{\rm S}$ and $R_{\rm S}$) gives a constraint on the dimensionless parameters $\eta_{\rm acc}$, $f_{\rm acc}$ and $f_{\rm c}$,

$$\eta_{\rm acc} f_{\rm acc} f_{\rm c}^{-9/2} \approx \left(\frac{M_{\rm S}}{10^5\,{\rm M}_\odot}\right)^{-1/4} \left(\frac{T_{\rm S}}{2.4\times10^4\,{\rm K}}\right)^4. \tag{19}$$

Replacing the SMS mass with the SMS radius and rescaling we find:

$$\eta_{\rm acc}\, f_{\rm acc}\, f_{\rm c}^{-5} = 0.4\times \left(\frac{T_{\rm S}}{1.8\times10^4\,{\rm K}}\right)^4 \left(\frac{R_{\rm S}}{5\times10^4\,{\rm R}_\odot}\right)^{-1/2}, \tag{20}$$

where we chose parameters that roughly match the spectra analysed in section 5. Eq. 20 must be valid for the recovered $T_{\rm S}$ and $R_{\rm S}$ to represent a physical SMS. Here we give some rough estimates for the values of $\eta_{\rm acc}$, $f_{\rm acc}$, and in particular discuss the possible range of $f_{\rm c}$.

From energy conservation we must have $\eta_{\rm acc} \leq 1$. Here we assume values close to unity, which correspond to full thermalisation of the accretion flow. By definition, $f_{\rm acc} < 1$ and we can express the following constraint:

$$f_{\rm acc} = (0.4 f_{\rm c}^5) \times \eta_{\rm acc}^{-1} \left(\frac{T_{\rm S}}{1.8\times10^4\,{\rm K}}\right)^4 \left(\frac{R_{\rm S}}{5\times10^4\,{\rm R}_\odot}\right)^{-1/2}, \tag{21}$$

where we used Eq. 15. The actual accretion rate scales instead as:

$$\dot{M}_{\rm S} \approx \left(2\times10^4 f_{\rm c}^2\right) \eta_{\rm acc}^{-1} \left(\frac{T_{\rm S}}{1.8\times10^4\,{\rm K}}\right)^4 \left(\frac{{\rm R}_{\rm S}}{5\times10^4\,R_\odot}\right) {\rm M}_\odot\,{\rm yr}^{-1}. \tag{22}$$

For convenience, we report it here also in terms of the SMS mass:

$$\dot{M}_{\rm S} \approx 10^4 f_{\rm c}^3 \eta_{\rm acc}^{-1} \left(\frac{T_{\rm S}}{1.8\times10^4\,{\rm K}}\right)^4 \left(\frac{{\rm M_S}}{10^4\,M_\odot}\right)^{1/2} {\rm M_\odot\,yr^{-1}}. \quad (23)$$

Note the strong dependence of the accretion rate (and fraction of the maximum rate) on the compression factor $f_{\rm c}$, to which we will return in section 6.

Estimating a plausible range for the compression factor is subtle since deviations from the mass radius relation of Eq.13 can have several causes. As stated in Hosokawa et al. (2010, 2012, 2013), SMS mass radius relations should be revised to account for the effect of ram pressure, which is expected to become meaningful as accretion rates are increased. In our specific case, we are by construction in a regime where the temperature (and thus, entropy) at the surface of the star is entirely dominated by the thermalisation of accreting gas, so we would expect compression. Furthermore, it is possible for details of the SMS internal structure under extreme accretion rates $\gtrsim 10^2$ M$_\odot$ yr^{-1} to cause evolution away from the Hayashi limit. The latter is simply a maximum theoretical value and stars over a wide range of mass decades typically are more compact and hotter (Stahler et al. 1980a,b, 1981; Kippenhahn & Weigert 1994). In particular, SMS have only been simulated robustly for accretion rates of up to a few M$_\odot$ yr^{-1}, and up to masses of $\lesssim 10^5$ M$_\odot$. One work attempting to push the accretion rates above $\sim 10^2$ M$_\odot$ found a clear, sudden increase in effective temperature at roughly constant luminosity for SMS with masses larger than 10^5 M$_\odot$, implying a reduction in radius of order ~ 10 (see the evolutionary tracks in Nandal et al. 2024; Nandal & Loeb 2025). Additionally, the only work that has modeled the formation of a SMS directly from angular momentum loss mechanisms in SMDs finds the central star-like object to be more compact than Eq. 13 by factors of 1 to 100, strongly depending on the density profile of the disc (Zwick et al. 2023). Finally, we note also that the definition of the stellar surface itself is subtle in a composite model of a stellar component plus a disc. In our particular case, $R_{\rm S}$ is best interpreted as the radius at which the majority of the accreting gas has thermalised and at which the bulk of the thermal radiation can escape the system. This may vary from typical definitions set by e.g. vanishing pressure or optical depth of order unity (Kippenhahn & Weigert 1994).

Because of these considerations, we opt to simply interpret $f_{\rm c}$ as a phenomenological modification to the typical SMS mass radius relation (Eq. 13), which is derived under the specific conditions detailed in Hosokawa et al. (2013). Therefore, we let its value vary from 0.01 to 1. As we will argue in section 5 and 6, additional constraints can be leveraged to estimate a value for $f_{\rm c}$ in the context of applying the SMS/SMD model to LRDs.

3.3. *GR instability*

The end of the life of a highly accreting SMS is triggered by the general relativistic instability Chandrasekhar (1964). The onset of the GR instability for highly accreting SMS has been studied in detail in several works, consistently finding a limit of $\sim 10^6$ M$_\odot$ for non-rotating SMS through a wide range of accretion rates (Nandal et al. 2024; Haemmerlé 2025). However, other forms of support such as rotation or magnetic fields can significantly postpone the collapse (Fowler 1966; Bisnovatyi-Kogan et al. 1967; Baumgarte & Shapiro 1999; Shibata et al. 2016; Haemmerlé et al. 2021; Nandal et al. 2024) and allow for order of magnitude larger SMS masses. When accretion onto the SMS is provided by a self-gravitating disc, we do expect rotational support to play an important role in delaying the onset of the GR instability. Therefore, we can expect SMSs of sizes up to $\sim 10^7$ M$_\odot$ to be stable.

4. MASSIVE SELF-GRAVITATING DISCS

4.1. *Disc radius, scale-height and temperature*

The formation of SMDs has been analysed in detail in several studies with high-resolution multi-scale simulations of high-z galaxy mergers, including from cosmological initial conditions (Mayer et al. 2010, 2015; Bonoli et al. 2014; Mayer & Bonoli 2019; Mayer et al. 2024). In the simulations, efficient dissipation of the merger's orbital kinetic energy via shocks and tidal torques leads to the formation of a compact SMD. The size of the disc is typically of order a pc and in the range $10^8 - 10^9 M_\odot$. This corresponds to roughly 10% of the total pre-merger gas in the galaxies. The SMDs that form are self-gravitating, with Toomre parameters in the range $1-2$ such that gravitational instabilities are expected to drive turbulence in the disc. The gravito-turbulence gives rise to super-thermal velocity dispersions in the range $10-20$% of the rotational velocity, resulting in disc aspect ratios ~ 0.1, exceeding those typically associated to such cold discs (e.g. $\sim 3000-6000$ K). Due to its high density, the SMD is optically thick with photon diffusion times exceeding the local orbital time, preventing the disc from fragmenting—except in the outermost low-density regions (see discussion in Mayer et al. 2015; Zwick et al. 2023)

Importantly, however, such simulations have only been carried out for highly massive galaxy mergers with a stellar mass of $\sim 10^{10}$ M$_\odot$. Here we assume that the general characteristics of SMD formation can be scaled to major galaxy mergers of smaller total mass. In short, we preserve that approximately 10% of the gas mass participates in the inflow, ultimately settling into a compact, self-gravitating disc of a similar temperature range with scale-heights supported by underlying turbulence. We characterise the disc geometry by a radius $R_{\rm D}$

and a scale-height $H_{\rm D}$ with typical aspect-ratio $h_{\rm D}$. At the largest scales

$$H_{\rm D} = h_{\rm D}\, R_{\rm D}, \tag{24}$$

and we enforce $h_{\rm D} < 1$ to preserve a thin geometry.

4.2. *Toomre stability*

The criterion for Toomre stability determines whether a disc is stabilised against fragmentation by its own shear (Toomre 1964). It is given by:

$$\mathcal{S} \equiv \frac{c_{\rm s}\kappa}{2\pi G\rho H_{\rm D}} > 1, \tag{25}$$

where κ is the epicyclic frequency, $c_{\rm s}$ the speed of sound and ρ the gas density. The epicyclic frequency is computed as:

$$\kappa^2 = \frac{2\Omega}{R}\frac{\rm d}{{\rm d}R}(R^2\Omega). \tag{26}$$

While formally this criterion is dependent on the disc's radial profile, we apply it here to estimate whether the disc as a whole can be sustained against global instabilities for a sufficient timescale. The bulk rotational frequency of the disc is $\Omega_{\rm D} = \sqrt{R_{\rm D}/(GM_{\rm D})}$, such that:

$$\kappa^2 \approx 2\frac{R_{\rm D}}{GM_{\rm D}}. \tag{27}$$

Expressing the stability criterion in terms of our system variables gives:

$$\mathcal{S} \approx 1.5 \times \left(\frac{h_{\rm D}}{10^{-2}} \cdot \frac{n_{\rm D}}{10^{14}\,{\rm cm^{-3}}}\right)^{-3/2} \times \left(\frac{R_{\rm d}}{0.1\,{\rm pc}}\right)^{-2} \left(\frac{T_{\rm D}}{4300\,{\rm K}}\right)^{1/2}, \tag{28}$$

where we assumed a monoatomic gas of pure hydrogen. To enforce this physical constraint, we will select disc solutions that have a nominal Toomre parameter of 1.5. Fixing the Toomre parameter gives a constraint on both the scale-height and density of the disc as a function of observable spectral parameters in our model.

4.3. *Accretion rates in self-gravitating discs*

In our model, the accretion rate onto the SMS is supplied by turbulent angular momentum transport in the SMD. In full generality, the accretion rate is given by:

$$\dot{M}_{\rm D} = 2\pi R_{\rm D}\rho H_{\rm D} v_{\rm r} \tag{29}$$

where $v_{\rm r}$ is the radial velocity of fluid elements through the disc. We formulate the radial inflow through the standard alpha prescription (Shakura & Sunyaev 1973) where:

$$v_r \sim \alpha c_s h_{\rm D}. \tag{30}$$

Then, the accretion rate becomes:

$$\dot{M} \sim \alpha 2\pi R_{\rm D}^2 \rho h_{\rm D}^2 c_s\,. \tag{31}$$

We enforce $\alpha < 1$ to exclude turbulent eddies larger than a scale-height or supersonic turn-over velocities. Evaluating for typical parameters gives:

$$\dot{M}_{\rm D} \approx 9.5 \times \left(\frac{\alpha\, h_{\rm D}^2}{10^{-5}} \cdot \frac{n_{\rm D}}{10^{14}\,{\rm cm^{-3}}}\right) \times \left(\frac{R_{\rm d}}{0.1\,{\rm pc}}\right)^2 \left(\frac{T_{\rm D}}{4300\,{\rm K}}\right)^{1/2} {\rm M_\odot\,yr^{-1}}. \tag{32}$$

Inverting Eq. 32 yields a constraint on the value of α:

$$\alpha \approx 0.1 \times \frac{\dot{M}}{10\,M_\odot\,{\rm yr^{-1}}} \left(\frac{h_{\rm D}^2}{10^{-4}} \cdot \frac{n_{\rm D}}{10^{14}\,{\rm cm^{-3}}}\right)^{-1} \times \left(\frac{R_{\rm d}}{0.1\,{\rm pc}}\right)^{-2} \left(\frac{T_{\rm D}}{4300\,{\rm K}}\right)^{-1/2}. \tag{33}$$

Values of $\alpha \sim 0.1$ are found to adequately fit observed AGN spectra (King et al. 2007). Similarly, in the case of a marginally stable gravito-turbulent disc with a Toomre parameter $\mathcal{S} \lesssim 2$, α is also typically found to be of order ~ 0.1 (Gammie 2001; Chen et al. 2023).

Given a value of α and a best fit spectral model, equating $\dot{M}_{\rm S} = \dot{M}_{\rm D}$ gives a constraint on the disc density and scale-height. Here we select disc solutions that have a nominal value of $\alpha = 0.2$, which corresponds to a maximally saturated gravito-turbulent effective viscosity (Chen et al. 2023).

4.4. *Line broadening*

In our model, warm hydrogen lines such as H_α and H_β are emitted by the bulk of the gas in the accretion disc. The circular velocity of the disc is given by:

$$v_{\rm D} = \sqrt{\frac{GM_{\rm D}}{R_{\rm D}}} \approx 2100\,{\rm km/s} \left(\frac{M_{\rm D}}{10^8\,{\rm M_\odot}}\right)^{1/2} \left(\frac{0.1\,{\rm pc}}{R_{\rm D}}\right)^{1/2}. \tag{34}$$

The corresponding line broadening at wavelength λ is typically described as a Gaussian with a standard deviation proportional to the circular velocity, projected onto the line of sight:

$$\sigma_\lambda = \sin(\iota)\frac{v_{\rm D}}{c}\lambda. \tag{35}$$

Therefore, fitting the broadening of the lines gives us another constraint on the disc parameters. The full set of constraints from line broadening, $\mathcal{S}$, α, and the spectral fit completely fixes the disc solution up to different choices of the SMS compression factor $f_{\rm c}$. As we will see in section 5, the disc density $n_{\rm D}$ can be recovered up to a scaling factor $\propto f_{\rm c}^{-2}$ and the aspect ratio $h_{\rm D}$ up to a factor $f_{\rm c}^2$.

5. MODEL FITTING TO OBSERVED SPECTRA

5.1. *Representative fits for J0647-1045 and COS-756434*

We demonstrate that the SMD/SMS model is able to reproduce observations, while also preserving the physical constraints detailed in section 2, by fitting a small number of spectra. LRD spectra are presented in several publications (e.g. Setton et al. 2024; Greene et al. 2024; Inayoshi et al. 2025). We select two based on the following criteria: They present with the characteristic spectral V-shape and broad Balmer emission lines, and they do not posses a strong Balmer-break (which is currently not modeled, though see section 6 for further discussion). Additionally, we prefer LRDs that have been observed at high SNR, with published spectra in plain units of flux. We choose two spectra that follow these criteria denoted as J0647-1045 (Killi et al. 2024) and COS-756434 (Akins et al. 2024) located at a redshift of 4.55 and 6.99. We perform a least-squares spectral fitting in log-space by employing Monte-Carlo Markhov-Chain (MCMC) methods via the `emcee` package (Foreman-Mackey et al. 2013), as detailed in Appendix A (which also includes the full posteriors for the recovered parameters). The fitting procedure accounts for the physical constraints detailed in sections 2, 3 and 4, as well as the presence of additional absorption and emission which are removed from the spectra to allow for better fitting of the continuum.

The best fit spectra for J0647-1045 and COS-756434 are shown in Fig. 3, and the best fit parameters that are fully constrained by the MCMC fitting are listed in Table 2. The 1-d posteriors of these parameters are roughly Gaussian, and we simply report their standard deviation as a measure of the uncertainty on the spectral fit (see Appendix A for the full posteriors). The SMD/SMD model provides an excellent fit to the observed spectra over the entire observed range, while also following the many physical constraints detailed in section 2. Additionally, it respects both higher- and lower-energy observational constraints. In the bottom panel of Fig. 3, we include with our fits upper-limits on the X-ray emission from stacked *Chandra* observations (Sacchi & Bogdan 2025) as well as infrared (IR) constraints from a particularly bright and nearby source which we take as upper-limits (Wang et al. 2025). However, we will see that accretion rates below the Eddington limit, and the preservation of a thin disc geometry require values of the compression parameter $f_c < 1$, which we will discuss in detail in the next section.

As expected, we recover temperatures of the order of $\sim$ 4000 K and 20000 K for the cold and the hot part of the spectrum, respectively. Additionally, the size ratio between the two BB components is of order $\sim$ 100, as implied by the relative flatness of the specific flux across the observed band. The required typical size to match the luminosity for the cold part of the spectrum is roughly $\sim$ 0.1 pc. We highlight this in particular, as a few works have tentatively associated this spectral feature with a hypothetical structure at the Hayashi limit (Inayoshi et al. 2024; Liu et al. 2025), similar to a SMS. However, by using Eq. 13 we can see that SMS following the Hayashi limit reach sizes of ~ 0.1 pc at a corresponding mass of $\sim f_c^{-2} \times 3 \times 10^8$ M$_\odot$. Since this is at least one to two orders of magnitude larger than the expected onset mass for the GR instability, we deem this interpretation to be implausible. Very recently Begelman & Dexter (2025) suggested that such a large structure may explained by a late-stage quasi-star, i.e. a bloated SMS envelope containing a massive BH, though other spectral features such as the UV peak are not treated in detail. Similarly, Nandal & Loeb (2025) invoke a SMS accreting at super-Eddington rates, attributing e.g. Balmer break features to details in the stellar atmosphere. Both models rely on extreme accretion rates to drive SMS formation and growth, though do not model the geometry and emission of the accretion flow itself. Instead, our model is closer to Zhang et al. (2025) which associates the cooler part of LRD spectra with the existence of a larger scale self-gravitating disc, while relying on a more standard AGN interpretation for line broadening[1].

	J0647-1045	COS-756434
z	4.55	6.99
T_S [K]	$(1.77 \pm .13) \times 10^4$	$(2.14 \pm .28) \times 10^4$
R_S [R$_\odot$]	$(6.76 \pm .93) \times 10^4$	$(6.80 \pm 1.51) \times 10^4$
T_D [K]	2800 ± 230	4500 ± 400
R_D [pc]	0.11 ± 0.03	0.06 ± 0.016
M_D [10^8 M$_\odot$]	2.0 ± 1.0	0.73 ± 0.38
ι	$19.6° \pm 3.8°$	$13.5° \pm 3.1°$

Table 2. Summary of the fully constrained best fit parameters and their uncertainties for the two given LRD spectra.

5.2. *Disc geometry, accretion rate and SMS mass*

Several additional physical parameters of J0647-1045 and COS-756434 are constrained up to a choice of the compression factor f_c. These are reported in Table 3. We highlight here some important considerations that are valid for both sources and use these to estimate reasonable values for f_c.

The geometry and density of the SMDs is fixed by by a choice of f_c. As discussed in section 4, marginally stable self-gravitating discs in proto-galaxies have typical scale-heights of $h_D \sim 0.01$ to ~ 0.1 (Lodato & Natarajan 2007; Mayer et al. 2010, 2015; Booth & Clarke 2019). Adding this constraint fixes values of $f_c \lesssim 0.1$. Additionally, it is important to note that no thin disc solutions with $h_D < 1$ are found for $f_c \gtrsim 0.4$ while preserving a Toomre parameter of $\mathcal{S} \sim 1.5$ and

[1] We note that out of the mentioned articles, only Zhang et al. (2025) clearly show well fitting continuum spectral models over the entire observed range.

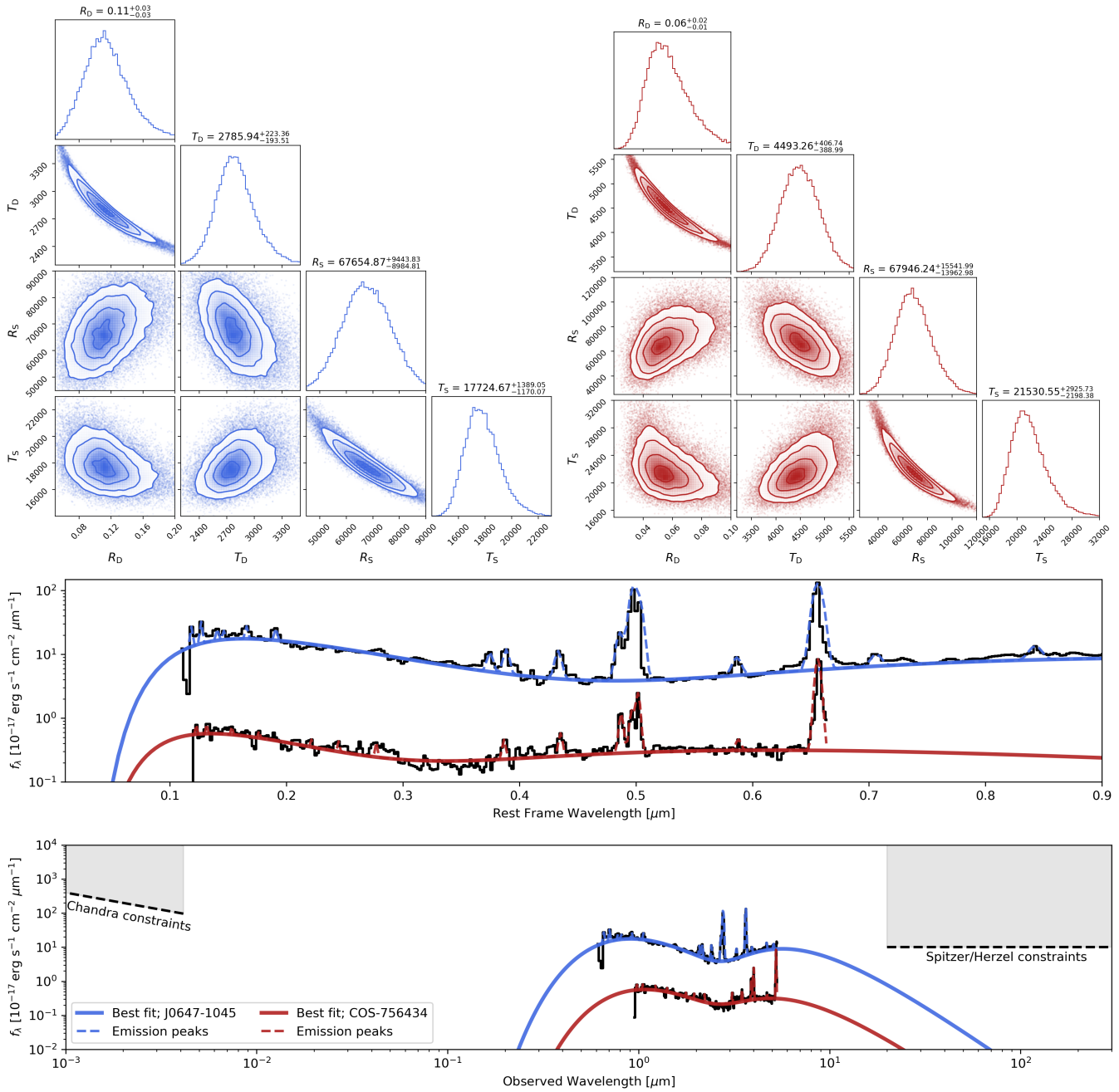

Figure 3. Plot of the best-fit model for J0647-1045 (blue) and COS-756434 (red). The top section shows a part of the recovered posteriors from the MCMC parameter fitting, highlighting a correlation between the SMS/SMD size and temperature. The bottom two panels show the resulting model spectra plotted over the observed data, including and excluding emission peaks. The constraints in the X-ray and IR are adapted from published work (Sacchi & Bogdan 2025; Wang et al. 2025).

a viscosity $\alpha \sim 0.1$ (the precise condition depends on a choice of the latter two parameters). The associated SMD densities are comparable to or lower than typical AGN densities of $\sim 10^{14}$ cm^{-3} (Shakura & Sunyaev 1973; Frank et al. 2002; Jiang et al. 2019) and do not provide further insights (beyond a potential connection to Balmer-breaks discussed in section 6). The recovered masses of the SMSs are comparable for both sources, $\sim (7 \times 10^4)\, f_c^{-2}$ M$_\odot$. Recall that the majority of estimates place the onset of the GR instability for SMSs at $\gtrsim 10^6$ M$_\odot$ (see section 3). Assuming a constant accretion rate, the timescale for an SMS to change mass considerably is $M_S/\dot{M}$ such that the longest phase of the entire SMS lifetime is just before the onset of the GR instability when the mass doubling timescale is longest. Consequently, the most likely time for an observer to see the system is also close to the maximum SMS mass. We find that a compression factor

	J0647-1045	COS-756434
M_S [10^4 $M_\odot$]	$(6.8 \pm 1.9) \times f_c^{-2}$	$(6.8 \pm 3.2) \times f_c^{-2}$
$\dot{M}$ [10^3 $M_\odot$ yr^{-1}]	$(25.8 \pm 4.6) \times f_c^2$	$(56 \pm 20) \times f_c^2$
n_D [10^{11} cm^{-3}]	$\sim 5 \times f_c^{-2}$	$\sim 0.6 \times f_c^{-2}$
h_D	$\sim 6.0 \times f_c^2$	$\sim 6.0 \times f_c^2$

Table 3. Summary of the additional best fit parameters that depend on f_c. Note that a value of $f_c < 1$ is required to preserve a thin disc geometry as well as sub-Eddington accretion rates. The entire SMS/SMD system, including disc geometry and inclination, is determined by spectral fitting up to a choice of f_c.

$f_c \lesssim 0.1$ gives a best fit SMS mass on the order of several 10^6 $M_\odot$, matching the expectations set by the GR instability limit. Finally, for the recovered parameters, the accretion rate through the disc and onto the SMS scales roughly as $\sim f_c^2 \times 10^4$ $M_\odot$ yr^{-1} (see Eq. 15). Imposing Eddington limited accretion (see Eq. 18) similarly—and consistently—requires a compression factor $f_c \lesssim 0.1$ corresponding to accretion rates $\lesssim 10^2$ $M_\odot$ yr^{-1}.

These three separate considerations lead us to postulate a value of $f_c \lesssim 0.1$. If such values are physical, the SMS/SMD model becomes entirely consistent with Eddington-limited accretion and turbulent angular momentum transport in thin, self-gravitating discs. Remarkably, the same choice for f_c will also be sufficient to roughly match the observed number density of LRDs and the expected galaxy mass – BH mass relation (as detailed in section 6).

Overall, the two sources for which we performed a full MCMC fitting show a remarkable similarity in the recovered best fit parameters. This is partly due to the surprisingly universal features of LRD spectra, and partly due to the extremely weak scaling of the SMS/SMD model with physical parameters (with the exception of the compression parameter f_c). We claim that the SMS/SMD model is able to adequately fit a large subset of LRD spectra. As seen in Fig. 2, slight differences in the spectra can be accounted for by the following: Luminosity and hardness variations in the hot part of the spectra can be attributed to varying the SMS component radius and temperature. Variation in the cold portion of the spectra can occur from varying disc inclination, size and temperature. Additionally, a combination of inclination, disc mass and disc radius can account for variations in the line broadening. Valid solutions that respect the constraints discussed in section 2 can always be found, though often require values of the compression parameter $f_c \lesssim 1$. The only major feature present in a significant subset of LRD spectra that the SMS/SMD model currently does directly address are the prominent Balmer breaks and absorption features seen in a subset of LRDs. These are discussed in more detail in section 6.

6. DISCUSSION

6.1. *Spectral features*

Our model of a SMS rapidly accreting from a SMD is able to faithfully capture the defining spectral characteristic of LRDs, namely the spectral-V in the rest-frame optical and UV emission. Beyond this core tenet, however, the model possesses a number of other potentially desirable properties which we discuss qualitatively within the full context of LRD observations.

Of particular note, in the AGN interpretation of LRDs, one of the most puzzling features is the near complete lack of X-ray emission (Yue et al. 2024; Sacchi & Bogdan 2025). At present these constraints appear to exclude existing appeals to X-ray obscuration (Maiolino et al. 2025), efficient Compton cooling (Madau & Haardt 2024), or steep spectral shapes in super-Eddington accreting SMBHs (Inayoshi et al. 2024; Pacucci & Narayan 2024). An accreting SMS, however, is highly extended, and as such would create no relevant X-rays (see Fig. 3).

Another unique feature of the Balmer emission in LRDs, is that many sources posses strong Balmer breaks—and in some cases decrements that are too large to explain with an evolved stellar component (Naidu et al. 2025)—as well as absorption features in the non-resonant Hα and Hβ lines. Because the $n = 2$ hydrogen levels that source these features are extremely short-lived, these features require large gas densities (Juodžbalis et al. 2024). While the required densities are generally consistent with typical AGN broad line regions (for characteristic ionization temperatures $\sim 10^4$K), Balmer absorption features are very rare in typical quasars (Aoki et al. 2006; Hall 2007; Schulze et al. 2018; Zhang et al. 2018).[2] This had led many authors to speculate that LRDs are AGN embedded in dense clouds of warm gas with covering factors near unity (Juodžbalis et al. 2024; Inayoshi & Maiolino 2025; Naidu et al. 2025; Kido et al. 2025). For cooler characteristic temperatures ($\sim$ 5000K), Liu et al. (2025) demonstrated that Balmer decrements (and by necessity, associated absorption features) remain prominent for photospheric gas densities $\lesssim 10^{-9}$g cm^{-3} with a "sweet spot" in the effective continuum opacity ratio[3] in the range $\sim 10^{-10} - 10^{-11}$g cm^{-3} (see e.g. their Figure 2). For compression values $f_c \lesssim 0.1$ as determined in Section 5, the characteristic densities of our SMDs fall precisely in this range (see Table 3), implying that such discs could self-consistently source Balmer breaks and absorption features. We comment that our model would predict those systems with Balmer features to have compara-

[2] Although we note that Balmer absorption features have been observed in 10-20% of AGN observed by JWST (Lin et al. 2024).

[3] The ratio of the effective opacity at 4000Å to that at 3600Å, straddling the Balmer decrement.

tively warm discs ($\gtrsim$ 4000K) and those without to be colder. However, the particulars of these processes would likely be sensitive to the details of the disc structure and turbulence (and may also emerge from associated accretion winds). We leave a more in-depth analysis for future work, but note that this intrinsic complexity might account for the variation in the presence, strength, and width of Balmer features, as well as the apparent range of absorption centroids from blue- to red-shifted relative to the line centres (Matthee et al. 2024; Labbe et al. 2024; Kocevski et al. 2024). We also note that a self-gravitating SMD naturally produces "over-broadened" Balmer lines relative to equivalent virial estimates because of the flatter rotation curve and larger velocities at comparable radius. In tandem with the intrinsic gravito-turbulence, this could account for the non-gaussian wings of the broad lines (Rusakov et al. 2025).

An originally prominent interpretation of LRDs was highly (or uniquely) dust-obscured AGN, but faint rest-frame near-infrared (NIR) observations suggest a generic lack of hot-dust tori (Eisenstein et al. 2023; Williams et al. 2024; Akins et al. 2024; Wang et al. 2025). In general, the LRDs tend to show a very flat rest-frame NIR component that is also inconsistent with un-obscured AGN (but may be compatible with a 1.6μm bump from star-formation; Sawicki 2002; Pérez-González et al. 2024). This emission, conversely, is well approximated by a blackbody spectrum with temperature of order 5000K (Inayoshi et al. 2025; Liu et al. 2025; Begelman & Dexter 2025) in qualitative agreement with the Rayleigh-Jeans tail of emission sourced by the SMD in our model.

6.2. *Rates and redshift evolution*

The number density of LRDs has been estimated to be of the order $\sim 10^{-5} - 10^{-4}$ Mpc^{-3} (Pérez-González et al. 2024; Matthee et al. 2024; Ma et al. 2025), with a distribution peaking around redshift $z \sim 5$ and distributed across $2 \lesssim z \lesssim 10$ (Kocevski et al. 2024). Here we start with a simple order of magnitude estimate for the expected number density of LRDs in our model. We then derive its redshift evolution in more detail. We assume that the parameters recovered from the J0647-1045 and COS-756434 spectral fitting are representative of the entire LRD population as discussed in section 5.

SMDs can be formed as a consequence of the large inflows triggered by a major galaxy merger. For our fitted LRD spectra, the recovered SMD masses are of the order $\sim 10^8$ M$_\odot$. As discussed in section 4, we only consider the merger of galaxies where this comprises $\sim 10\%$ of the gas. At $z \sim 5$ and above, the gas mass in galaxies is typically larger than the stellar mass by almost an order of magnitude (see e.g. Tacconi et al. 2018; Wiklind et al. 2019; Heintz et al. 2022). Therefore, we use the merger rate of galaxies with a stellar mass of $\gtrsim 10^8$ M$_\odot$, which corresponds to a total gas mass of $\sim 10^9$ M$_\odot$, as a simple proxy for those with sufficient gas to form a SMD. Note that mergers of larger galaxies may also form larger SMDs which perhaps could model particularly luminous LRDs, though these would be subdominant in rate. In fact, the distribution of sizes of SMDs can be predicted within the scenario of galaxy mergers, which we leave to future work.

In the appropriate redshift range, the number density of galaxies with at least 10^8 M$_\odot$ in stars is (Song et al. 2016; McLeod et al. 2021):

$$n_8^{\rm gal} \approx 10^{-2} \text{ to } 10^{-1}\,\text{Mpc}^{-3}. \tag{36}$$

Between redshifts $\sim 4-8$ (where the majority of LRDs are observed), the rate of major mergers per galaxy is approximately 1 Gyr^{-1}, where we define a major merger to have a mass ratio of $\gtrsim 0.25$ (Stewart et al. 2009; Rodriguez-Gomez et al. 2015; O'Leary et al. 2021). Therefore, approximately every relevant galaxy will have undergone a major merger within this redshift range, and had the chance to form a SMD.

In our model LRDs are a transient stage that lasts approximately one SMS lifetime $\mathcal{T}_{\rm S}$, i.e. the total amount of time it takes for the star to grow and eventually collapse. We can then estimate the density of observed LRDs to be:

$$n_{\rm LRD} \approx n_8^{\rm gal} \times \frac{\mathcal{T}_{\rm S}}{1\,\text{Gyr}}, \tag{37}$$

where the Gyr in the denominator is approximately the time between $z = 8$ and $z = 4$, i.e. an appropriate redshift range. From Eq. 37, we deduce that the observed LRD number density is recovered for typical SMS lifetimes of order 10^6 yr.

As discussed in section 5, we assume that we are observing the SMS in the same mass decade in which they reach the maximum allowed mass. Using Eq. 15, the SMS lifetime is then approximately given by a mass doubling timescale:

$$\mathcal{T}_{\rm S} \approx \frac{M_{\rm S}}{\dot{M}_{\rm S}} \tag{38}$$

$$\approx 10^6 \times \left(\frac{f_{\rm c}}{0.05}\right)^{-4} \left(\frac{T_{\rm S}}{1.7\times10^4\,\text{K}}\right)^{-4} \left(\frac{R_{\rm S}}{7\times10^4\,\text{R}_\odot}\right) \text{yr} \tag{39}$$

where we inserted the best-fit values of J0647-1045. Note the very strong scaling with $f_{\rm c}$ and the fact that the required value is remarkably close to our estimates based on the accretion disc geometry and the Eddington limit detailed in section 5. If such values are physical, the proposed formation pathway for the SMS/SMD model can adequately reproduce the observed number density of LRDs. We also comment that the timescale for the SMS collapse after it becomes unstable, i.e. the free fall timescale, is approximately $1 - 10$ yr. Therefore, we would expect approximately 1 in 10^5 LRD to collapse into AGN while being observed.

The distribution of LRDs as a function of redshift can be derived in more detail from our model, as it exactly follows the major merger rate for galaxies with sufficient gas mass. We present here an estimate based on the halo merger rate from the Millennium simulation (Fakhouri et al. 2010):

$$\frac{\mathrm{d}^2\Gamma}{\mathrm{d}\xi \mathrm{d}z} = B_1 \left(\frac{M_\mathrm{h}}{10^{12}\,\mathrm{M}_\odot}\right)^{b_1} \xi^{b_2} \exp\left[\left(\frac{\xi}{B_2}\right)^{b_3}\right] (1+z)^{b_4}, \quad (40)$$

where Γ is the total number of mergers for a single dark matter halo of mass M_h, $\xi \leq 1$ is the halo merger mass ratio, and the best fit parameters are $[B_1, B_2, b_1, b_2, b_3, b_4] = [0.0104, 9.72 \times 9.72, 0.133, -1.995, 0.263, 0.0993]$. The merger rate per co-moving volume is found by multiplying the halo merger rate with the halo mass function. We use the parametrisation proposed by Tinker et al. (2008):

$$\frac{\mathrm{d}n}{\mathrm{d}M_\mathrm{h}} = f(\sigma)\frac{\rho_m}{M_\mathrm{h}}\frac{\mathrm{d}\log\sigma^{-1}}{\mathrm{d}M_\mathrm{h}}, \quad (41)$$

where σ^2 is an average over the density power spectrum, f a function describing the likelihood of a region to random-walk into being over the critical density, and ρ_m is the mean density of the universe. We use the best fit parameters reported in Tinker et al. (2008) for a value of the over-density $\Delta = 200$, which best reproduces a universal result. Note that we assume standard Λ-CDM cosmology with $\Omega_\mathrm{m} = 0.27$ and $\Omega_\Lambda = 0.73$. From this point, the halo merger rate can be related to the galaxy merger rate by a halo mass–galaxy mass relation. We use a fit of the stellar mass to halo mass ratio $\mathscr{F}^\star$ (Moster et al. 2018; Girelli et al. 2020):

$$\mathscr{F}^\star(M_\mathrm{h}) = 2D_1(1+z)^{\delta_1}\left[\left(\frac{M_\mathrm{h}}{D_2}\right)^{-\beta} + \left(\frac{M_\mathrm{h}}{D_2}\right)^{\gamma}\right]^{-1}, \quad (42)$$

$$D_2 = 10^{\delta_2 + z\delta_3}\,\mathrm{M}_\odot,$$
$$\beta = z\delta_4 + \delta_5,$$
$$\gamma = \delta_6(1+z)^{\delta_7},$$

where the best fit parameters are $[D_1, \delta_1, \delta_2, \delta_3, \delta_4, \delta_5, \delta_6, \delta_7] = [0.046, -0.38, 11.79, 0.20, 0.043, 0.96, 0.709, -0.18]$. Finally, we use a simple fit for the gas mass to stellar mass fraction provided in (Tacconi et al. 2018), which roughly increases with redshift as $(1+z)^{2.5}$. Collecting all of these ingredients, we obtain a differential merger rate $\mathcal{R}$ of the form:

$$\mathcal{R} \equiv \mathcal{R}(M_\mathrm{gas/gal}, \xi_\mathrm{gas/gal}, z)\ \left[\mathrm{Mpc}^{-3}\,\mathrm{Gyr}^{-1}\right], \quad (43)$$

which we can evaluate for either a certain gas mass or stellar mass, as well as for a certain mass ratio.

Fig. 4 shows a comparison of the differential merger rate for galaxies with a stellar (blue) or gas (red) mass of 10^8 $\mathrm{M}_\odot$, 10^9 $\mathrm{M}_\odot$ and 10^{10} $\mathrm{M}_\odot$. The rates are normalised, and shown for a galaxy mass ratio of 1. While we leave a thorough rate calculation as a function of galaxy mass and mass ratio for future work, we note that the distribution in redshift accurately matches the observed LRD distribution for galaxies in the relevant gas mass range. The early peak, at z$\sim$ 5, is due to the fact that galactic gas supply is progressively consumed in star formation such that less gas rich galaxies are available to merge as cosmic time progresses. The preliminary results displayed in Fig. 4 strongly suggest a connection between gas rich galaxy mergers and the redshift distribution of LRDs.

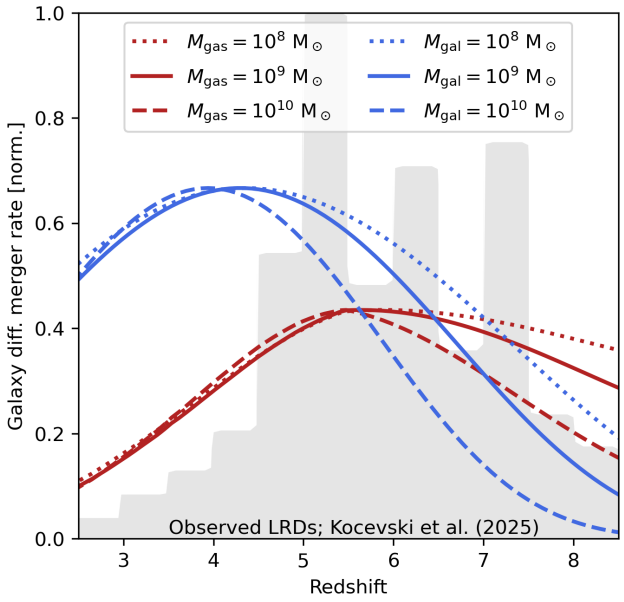

Figure 4. Comparison between the differential merger rates of galaxies with a certain stellar (blue) or gas (red) mass (see text) for a mass ratio of 1. The curves are generally normalised to correspond with the high redshift tail for the observed LRD distribution (in gray, Kocevski et al. 2025), and different gas (stellar) mass rates are normalized to share the same maximum. Note howmthe shape of the red curves match the entire observed distribution, strongly suggesting a connection between LRDs and gas rich galaxy mergers with masses $\gtrsim 10^8$ $\mathrm{M}_\odot$.

6.3. *Scaling relations and additional considerations*

Whereas SMBHs in the local universe typically comprise about $\sim$ 0.1% of their host galaxy mass (Magorrian et al. 1998; Reines & Volonteri 2015), the estimated masses of SMBHs in LRDs can be as high as $\gtrsim$ 10% (Harikane et al. 2023; Greene et al. 2024; Kocevski et al. 2024) with estimates based on assuming the existence of an AGN broad line region. While the intrinsic scatter of galaxy mass–BH mass relations grows with redshift (Hirschmann et al. 2010), such over-massive BHs would represent extreme outliers and pose additional challenges for standard galaxy–BH co-evolution (Habouzit et al. 2022). The line broadening in our model is set by the size and mass of the SMD rather than a pre-existing

BH component, and the BH mass resulting from the collapse of the central SMS is significantly smaller. Taking a reference value of $f_c \sim 0.1$, we recover SMS masses of a few 10^6 $M_\odot$ from our two representative spectral fits (see section 5). Assuming that the majority of the SMS is retained during the collapse, we expect a BH to be formed at comparable mass. The collapse takes place within a recently merged galaxy with at least a stellar mass of several 10^8 $M_\odot$ and a total gas mass of order 10^9 $M_\odot$, where efficient post-merger star formation is taking place (Hopkins et al. 2013; Capelo et al. 2015). Taking these reference values, we see that the predicted BH mass in the SMS/SMD model for LRDs is of order $\sim 0.1\%$ to $\sim 1\%$ of its galactic host, landing squarely in the expected range.

Finally, we highlight the recent analysis performed in Chen et al. (2025), in which the authors find constraints on the stellar mass of LRD hosts. The recovered constraints broadly imply that typical LRD hosts have stellar masses below few times $10^8 - 10^9$ $M_\odot$, where the only constrained galactic component has $10^{8.6}$ $M_\odot$. This perfectly matches with the formation pathway discussed in section 6.2. It is particularly intriguing that a majority of the LRDs in the analysis showcase off-centre emission, which does not have a clear interpretation. We speculate that the off-centre emission is a natural result of the galaxy merger, whereby galactic gas clouds collide upon first passage, but the stellar component relaxes over much longer timescales. This is the proposed mechanism of the recently discovered Infinity Galaxy (van Dokkum et al. 2025) in which a direct collapse event is speculated to have occurred.

7. SUMMARY AND CONCLUSIONS

In this work, we have presented a new physical interpretation of LRDs based on a SMS embedded within a self-gravitating accretion disc (SMD). The SMS/SMD model accounts for a number of key observational features of LRDs, including:

- The two-blackbody continuum shape underlying the V-shaped spectra.
- The observed broad Balmer emission lines, from the high rotational velocities in the SMD.
- The lack of significant X-ray and IR emission, without invoking additional obscuration.
- The observed redshift distribution of LRDs, from the distribution of gas-rich major galaxy mergers.
- Constraints on the size of LRD galactic hosts.

A key component of the model is the introduction of a phenomenological compression factor f_c, which parametrises a deviation from the SMS mass–radius relation of Hosokawa et al. (2013). If a compression ($f_c \lesssim 0.1$) is assumed, the model yields long system lifetimes sufficient to explain the observed number density of LRDs. Additionally, the model is consistent with sub-Eddington accretion, standard disc geometry, and varied Balmer emission/absorption behaviour. The predicted post-direct-collapse BH masses also land squarely within standard galaxy mass – BH mass relations. All parameters of the SMS/SMD system, including its inclination, can be determined by spectral fitting [in addition to a choice of f_c.

We envision two natural follow-ups this work: First, to thoroughly study the relationship between galaxy merger rates and expected distributions of LRD properties, including a more extensive series of spectral fits that include Balmer breaks. Second, to expand the range of simulations of highly accreting SMS in order to more precisely quantify the SMS mass–radius relation of SMS with $M_S \gtrsim 10^6$ $M_\odot$, beyond the several arguments presented in section 3. Such works would strongly establish the plausibility of the SMS/SMD model for LRDs. Together with the arguments presented here, this would bastion the claim that JWST may be directly observing SMS at the verge of relativistic instability: The stage just prior to the formation of the original SMBH seeds in the universe.

ACKNOWLEDGMENTS

L.Z. is supported by the Villum Fonden grant No. 29466, and by the ERC Starting Grant no. 101043143 – BlackHoleMergs. C.T. acknowledges support from the European Union's Horizon 2023 research and innovation program under Marie Sklodowska-Curie grant agreement No. 101148364. L.M. acknowledges support from the Swiss National Science Foundation under the Grant 200020-207406. L.Z. and C.T. thank János Takátsy and Daniel J. D'Orazio for marginally stable discussions. L.M. and C.T. thank Piero Madau, Naoki Yoshida, John Silverman and Zoltan Haiman for useful discussions on LRDs.

APPENDIX

A. DETAILS OF THE MCMC

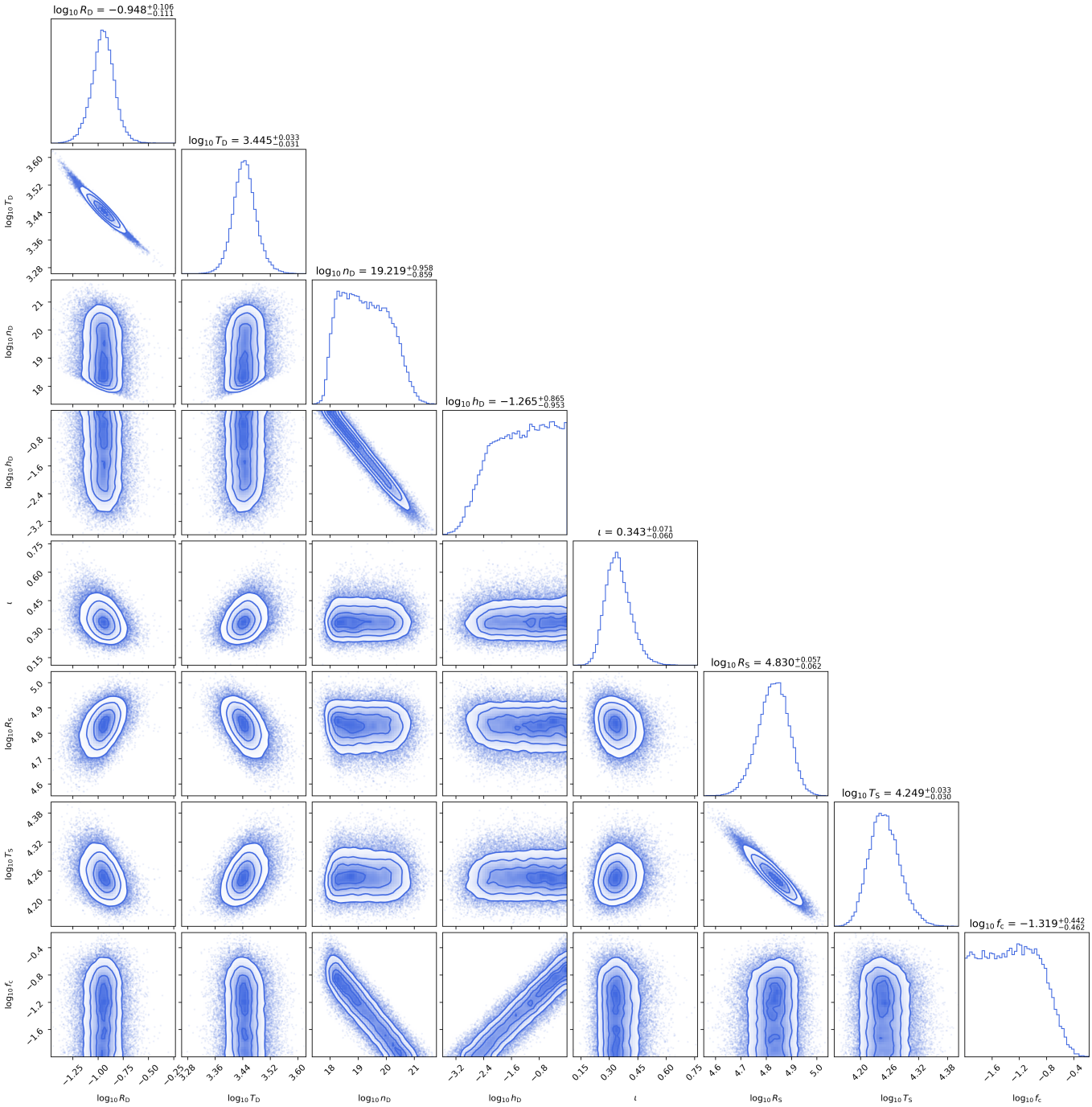

Figure 5. Full posterior for J0647-1045. The units for the parameters $[R_{\rm D}, T_{\rm D}, n_{\rm D}, h_{\rm D}, \iota, R_{\rm S}, T_{\rm S}, f_{\rm c}]$ are [pc,K,m^{-3},−,rad,R$_\odot$,K,−].

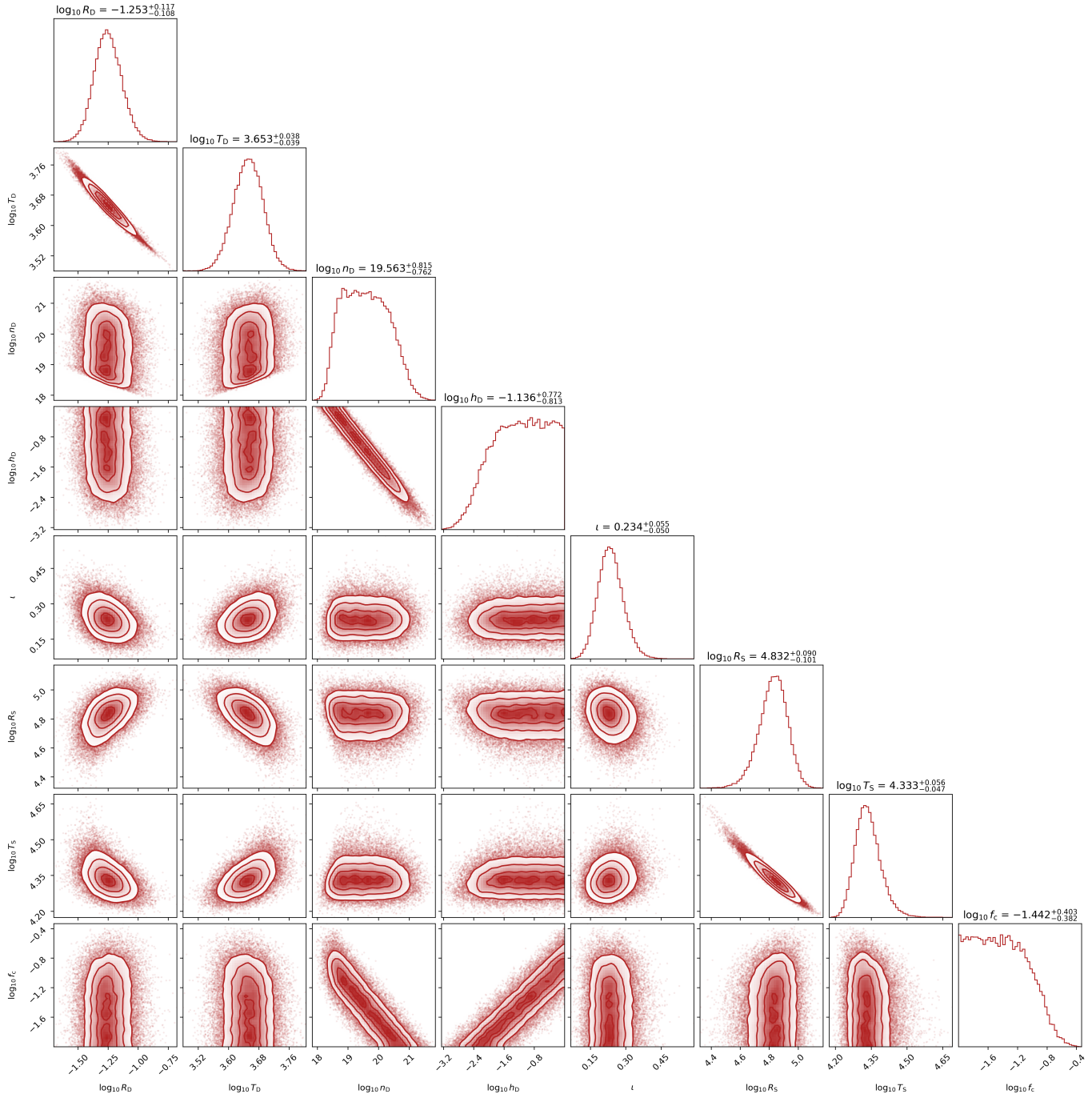

Figure 6. Full posterior for COS-756434. The units for the parameters $[R_{\rm D}, T_{\rm D}, n_{\rm D}, h_{\rm D}, \iota, R_{\rm S}, T_{\rm S}, f_{\rm c}]$ are [pc,K,m^{-3},−,rad,R$_\odot$,K,−].

We use Monte-Carlo-Markhov-Chain (MCMC) methods to perform the spectral fitting and estimate parameter correlations numerically. We define a likelihood function $\mathcal{L}$ of the form:

$$\mathcal{L}\left(\Theta\right) \propto \exp\left[-\left(S(\Theta) - D\right)^2\right], \tag{A1}$$

where $\Theta = [R_{\rm D}, T_{\rm D}, n_{\rm D}, h_{\rm D}, \iota, R_{\rm S}, T_{\rm S}, f_{\rm c}]$ are the parameters used to evaluate the spectral model S. The vector D represents the spectral data of a given LRD, taken with the NIR cam instrument of JWST (201 2016), where the total length is given by the spectral range of the measurement divided by the spectral resolution of the instrument (approximately 0.013 μm). In practice, we

used the data plotted in Killi et al. (2024) and Akins et al. (2024) for the spectra of J0647-1045 and COS-756434, respectively. Since no errors are given, we treat each data point as being equally weighted and independent.

We use the affine invariant sampler `emcee` (Foreman-Mackey et al. 2013) to perform the numerical tests, running 24 parallel walkers for approximately 20'000 to 30'000 steps. The typical auto-correlation time of the walkers is $\sim$ 200. We initialise the walkers by approximately fitting the spectra by eye. The burn-in to find the true maximum of the likelihood required approximately 500 steps and is removed. The priors for the perturbation parameters are initially flat in log-space. The exception is the inclination ι, which has a flat prior ranging from 0 to $\pi/4$. We implement several additional prior constraints on the recovered model parameters in order to enforce the physics discussed in section 2. The prior constraints are as follows:

- The SMS maximum accretion rate cannot be exceeded, i.e. $f_{\rm acc} < 1$.
- The disc must be stable, i.e. $\mathcal{S} > 1$.
- The accretion rate must respect turbulent angular momentum transport in the disc, i.e. $\alpha < 1$.

Additionally, we strongly prefer fits that correspond to Toomre parameters of $\mathcal{S} \sim 1.5$ and viscosity prescriptions of $\alpha \sim 0.1$. These are implemented as a Gaussian prior on $\mathcal{S}$ with a standard deviation of 0.25, and a Gaussian prior on $\log_{10}\,\alpha$ with a standard deviation of 0.25. The choices for the standard deviations are arbitrary beyond being numerically convenient and do not strongly influence the uncertainties in the recovered parameters, since these are dominated by other correlations.

In order to accurately fit the basic SMS/SMD spectral model to the data, we have to account for the various emission and absorption features. Emission and absorption peaks are identified in the data via the `scipy.findpeaks` function and added automatically to the spectral model as Gaussians. They do not provide any additional constraining power beyond the line broadening, which is fitted exclusively for the H_α, H_β and OIII lines. We show the full posteriors for J0647-1045 and COS-756434 in Figs. 5 and 6, respectively.

REFERENCES

2016, JWST User Documentation (JDox), JWST User Documentation Website

Abel, T., Bryan, G. L., & Norman, M. L. 2002, Science, 295, 93, doi: 10.1126/science.295.5552.93

Agarwal, B., Khochfar, S., Johnson, J. L., et al. 2012, MNRAS, 425, 2854, doi: 10.1111/j.1365-2966.2012.21651.x

Agarwal, B., Smith, B., Glover, S., Natarajan, P., & Khochfar, S. 2016, MNRAS, 459, 4209, doi: 10.1093/mnras/stw929

Akins, H. B., Casey, C. M., Lambrides, E., et al. 2024, arXiv e-prints, arXiv:2406.10341, doi: 10.48550/arXiv.2406.10341

Alvarez, M. A., Wise, J. H., & Abel, T. 2008, in American Institute of Physics Conference Series, Vol. 990, First Stars III, ed. B. W. O'Shea & A. Heger, 432–434, doi: 10.1063/1.2905657

Ananna, T. T., Bogdán, Á., Kovács, O. E., Natarajan, P., & Hickox, R. C. 2024, ApJL, 969, L18, doi: 10.3847/2041-8213/ad5669

Antonucci, R. 1993, ARA&A, 31, 473

Aoki, K., Iwata, I., Ohta, K., et al. 2006, ApJ, 651, 84, doi: 10.1086/507438

Baumgarte, T. W., & Shapiro, S. L. 1999, ApJ, 526, 941, doi: 10.1086/308006

Begelman, M. C. 2008, in American Institute of Physics Conference Series, Vol. 990, First Stars III, ed. B. W. O'Shea & A. Heger, 489–493, doi: 10.1063/1.2905669

Begelman, M. C. 2010, MNRAS, 402, 673, doi: 10.1111/j.1365-2966.2009.15916.x

Begelman, M. C., & Dexter, J. 2025, arXiv e-prints, arXiv:2507.09085, doi: 10.48550/arXiv.2507.09085

Begelman, M. C., Volonteri, M., & Rees, M. J. 2006, MNRAS, 370, 289, doi: 10.1111/j.1365-2966.2006.10467.x

Bellomo, N., Bernal, J. L., Raccanelli, A., & Verde, L. 2018, JCAP, 2018, 004, doi: 10.1088/1475-7516/2018/01/004

Bisnovatyi-Kogan, G. S., Zel'dovich, Y. B., & Novikov, I. D. 1967, Soviet Ast., 11, 419

Bogdán, Á., Goulding, A. D., Natarajan, P., et al. 2024, Nature Astronomy, 8, 126, doi: 10.1038/s41550-023-02111-9

Bolton, J. G., Gardner, F. F., & Mackey, M. B. 1963, Nature, 199, 682, doi: 10.1038/199682b0

Bonoli, S., Mayer, L., & Callegari, S. 2014, MNRAS, 437, 1576, doi: 10.1093/mnras/stt1990

Booth, R. A., & Clarke, C. J. 2019, MNRAS, 483, 3718, doi: 10.1093/mnras/sty3340

Capelo, P. R., Volonteri, M., Dotti, M., et al. 2015, MNRAS, 447, 2123, doi: 10.1093/mnras/stu2500

Chandrasekhar, S. 1964, ApJ, 140, 417, doi: 10.1086/147938

Chen, C.-H., Ho, L. C., Li, R., & Zhuang, M.-Y. 2025, ApJ, 983, 60, doi: 10.3847/1538-4357/ada93a

Chen, Y.-X., Jiang, Y.-F., Goodman, J., & Ostriker, E. C. 2023, ApJ, 948, 120, doi: 10.3847/1538-4357/acc023

Chon, S., Hosokawa, T., & Yoshida, N. 2018, MNRAS, 475, 4104, doi: 10.1093/mnras/sty086

Colgate, S. A., Cen, R., Li, H., Currier, N., & Warren, M. S. 2003, ApJL, 598, L7, doi: 10.1086/380426

Ding, X., Silverman, J. D., & Onoue, M. 2022, ApJL, 939, L28, doi: 10.3847/2041-8213/ac9c02

Eddington, A. S. 1921, Zeitschrift fur Physik, 7, 351, doi: 10.1007/BF01332806

Eisenstein, D. J., Willott, C., Alberts, S., et al. 2023, arXiv e-prints, arXiv:2306.02465, doi: 10.48550/arXiv.2306.02465

Fakhouri, O., Ma, C.-P., & Boylan-Kolchin, M. 2010, MNRAS, 406, 2267, doi: 10.1111/j.1365-2966.2010.16859.x

Fiacconi, D., & Rossi, E. M. 2016, MNRAS, 455, 2, doi: 10.1093/mnras/stv2237

Foreman-Mackey, D., Hogg, D. W., Lang, D., & Goodman, J. 2013, PASP, 125, 306, doi: 10.1086/670067

Fowler, W. A. 1966, ApJ, 144, 180, doi: 10.1086/148594

Frank, J., King, A., & Raine, D. J. 2002, Accretion Power in Astrophysics: Third Edition

Gammie, C. F. 2001, ApJ, 553, 174, doi: 10.1086/320631

Girelli, G., Pozzetti, L., Bolzonella, M., et al. 2020, A&A, 634, A135, doi: 10.1051/0004-6361/201936329

Greene, J. E., Labbe, I., Goulding, A. D., et al. 2024, ApJ, 964, 39, doi: 10.3847/1538-4357/ad1e5f

Habouzit, M., Volonteri, M., Latif, M., Dubois, Y., & Peirani, S. 2016, MNRAS, 463, 529, doi: 10.1093/mnras/stw1924

Habouzit, M., Onoue, M., Bañados, E., et al. 2022, MNRAS, 511, 3751, doi: 10.1093/mnras/stac225

Haemmerlé, L. 2020, A&A, 644, A154, doi: 10.1051/0004-6361/202039828

—. 2021, A&A, 650, A204, doi: 10.1051/0004-6361/202140893

—. 2025, arXiv e-prints, arXiv:2503.01970, doi: 10.48550/arXiv.2503.01970

Haemmerlé, L., Klessen, R. S., Mayer, L., & Zwick, L. 2021, A&A, 652, L7, doi: 10.1051/0004-6361/202141376

Haemmerlé, L., Woods, T. E., Klessen, R. S., Heger, A., & Whalen, D. J. 2018a, MNRAS, 474, 2757, doi: 10.1093/mnras/stx2919

—. 2018b, ApJL, 853, L3, doi: 10.3847/2041-8213/aaa462

Haiman, Z. 2013, in Astrophysics and Space Science Library, Vol. 396, The First Galaxies, ed. T. Wiklind, B. Mobasher, & V. Bromm, 293, doi: 10.1007/978-3-642-32362-1_6

Hall, P. B. 2007, AJ, 133, 1271, doi: 10.1086/511272

Harikane, Y., Zhang, Y., Nakajima, K., et al. 2023, ApJ, 959, 39, doi: 10.3847/1538-4357/ad029e

Hayashi, C. 1961, PASJ, 13, 450

Heintz, K. E., Oesch, P. A., Aravena, M., et al. 2022, ApJL, 934, L27, doi: 10.3847/2041-8213/ac8057

Herrington, N. P., Whalen, D. J., & Woods, T. E. 2023, MNRAS, 521, 463, doi: 10.1093/mnras/stad572

Hirano, S., Hosokawa, T., Yoshida, N., et al. 2014, ApJ, 781, 60, doi: 10.1088/0004-637X/781/2/60

Hirschmann, M., Khochfar, S., Burkert, A., et al. 2010, MNRAS, 407, 1016, doi: 10.1111/j.1365-2966.2010.17006.x

Hopkins, P. F., Cox, T. J., Hernquist, L., et al. 2013, MNRAS, 430, 1901, doi: 10.1093/mnras/stt017

Hosokawa, T., Omukai, K., & Yorke, H. W. 2012, ApJ, 756, 93, doi: 10.1088/0004-637X/756/1/93

Hosokawa, T., Yorke, H. W., Inayoshi, K., Omukai, K., & Yoshida, N. 2013, ApJ, 778, 178, doi: 10.1088/0004-637X/778/2/178

Hosokawa, T., Yorke, H. W., & Omukai, K. 2010, ApJ, 721, 478, doi: 10.1088/0004-637X/721/1/478

Huško, F., Lacey, C. G., Roper, W. J., et al. 2025, MNRAS, 537, 2559, doi: 10.1093/mnras/staf146

Inayoshi, K., Kimura, S. S., & Noda, H. 2024, arXiv e-prints, arXiv:2412.03653, doi: 10.48550/arXiv.2412.03653

Inayoshi, K., & Maiolino, R. 2025, ApJL, 980, L27, doi: 10.3847/2041-8213/adaebd

Inayoshi, K., Shangguan, J., Chen, X., Ho, L. C., & Haiman, Z. 2025, arXiv e-prints, arXiv:2505.05322, doi: 10.48550/arXiv.2505.05322

Jiang, J., Fabian, A. C., Dauser, T., et al. 2019, MNRAS, 489, 3436, doi: 10.1093/mnras/stz2326

Johnson, J. L., & Dijkstra, M. 2017, A&A, 601, A138, doi: 10.1051/0004-6361/201630010

Juodžbalis, I., Ji, X., Maiolino, R., et al. 2024, MNRAS, 535, 853, doi: 10.1093/mnras/stae2367

Kido, D., Ioka, K., Hotokezaka, K., Inayoshi, K., & Irwin, C. M. 2025, arXiv e-prints, arXiv:2505.06965, doi: 10.48550/arXiv.2505.06965

Killi, M., Watson, D., Brammer, G., et al. 2024, A&A, 691, A52, doi: 10.1051/0004-6361/202348857

King, A. R., Pringle, J. E., & Livio, M. 2007, MNRAS, 376, 1740, doi: 10.1111/j.1365-2966.2007.11556.x

Kippenhahn, R., & Weigert, A. 1994, Stellar Structure and Evolution, XVI, 468 pp. 192 figs.. Springer-Verlag Berlin Heidelberg New York. Also Astronomy and Astrophysics Library, -1

Kiyuna, M., Hosokawa, T., & Chon, S. 2024, MNRAS, 534, 3916, doi: 10.1093/mnras/stae2380

Kocevski, D. D., Finkelstein, S. L., Barro, G., et al. 2024, arXiv e-prints, arXiv:2404.03576, doi: 10.48550/arXiv.2404.03576

—. 2025, ApJ, 986, 126, doi: 10.3847/1538-4357/adbc7d

Koushiappas, S. M., Bullock, J. S., & Dekel, A. 2004, MNRAS, 354, 292, doi: 10.1111/j.1365-2966.2004.08190.x

Kroupa, P., Subr, L., Jerabkova, T., & Wang, L. 2020, MNRAS, 498, 5652, doi: 10.1093/mnras/staa2276

Labbe, I., Greene, J. E., Matthee, J., et al. 2024, arXiv e-prints, arXiv:2412.04557, doi: 10.48550/arXiv.2412.04557

Lambas, D. G., Alonso, S., Mesa, V., & O'Mill, A. L. 2012, A&A, 539, A45, doi: 10.1051/0004-6361/201117900

Latif, M. A., Schleicher, D. R. G., Schmidt, W., & Niemeyer, J. C. 2013, MNRAS, 436, 2989, doi: 10.1093/mnras/stt1786
Latif, M. A., Whalen, D. J., Khochfar, S., Herrington, N. P., & Woods, T. E. 2022, Nature, 607, 48, doi: 10.1038/s41586-022-04813-y
Lin, X., Wang, F., Fan, X., et al. 2024, ApJ, 974, 147, doi: 10.3847/1538-4357/ad6565
Liu, H., Jiang, Y.-F., Quataert, E., Greene, J. E., & Ma, Y. 2025, arXiv e-prints, arXiv:2507.07190, doi: 10.48550/arXiv.2507.07190
Lodato, G., & Natarajan, P. 2006, MNRAS, 371, 1813, doi: 10.1111/j.1365-2966.2006.10801.x
—. 2007, MNRAS, 377, L64, doi: 10.1111/j.1745-3933.2007.00304.x
Lupi, A., Haardt, F., Dotti, M., et al. 2016, MNRAS, 456, 2993, doi: 10.1093/mnras/stv2877
Lyke, B. W., Higley, A. N., McLane, J. N., et al. 2020, ApJS, 250, 8, doi: 10.3847/1538-4365/aba623
Ma, Y., Greene, J. E., Setton, D. J., et al. 2025, arXiv e-prints, arXiv:2504.08032, doi: 10.48550/arXiv.2504.08032
Madau, P., & Haardt, F. 2024, ApJL, 976, L24, doi: 10.3847/2041-8213/ad90e1
Madau, P., & Rees, M. J. 2001, ApJL, 551, L27, doi: 10.1086/319848
Magorrian, J., Tremaine, S., Richstone, D., et al. 1998, AJ, 115, 2285
Maiolino, R., Risaliti, G., Signorini, M., et al. 2025, MNRAS, 538, 1921, doi: 10.1093/mnras/staf359
Matthee, J., Naidu, R. P., Brammer, G., et al. 2024, ApJ, 963, 129, doi: 10.3847/1538-4357/ad2345
Mayer, L., & Bonoli, S. 2019, Reports on Progress in Physics, 82, 016901, doi: 10.1088/1361-6633/aad6a5
Mayer, L., Capelo, P. R., Zwick, L., & Di Matteo, T. 2024, ApJ, 961, 76, doi: 10.3847/1538-4357/ad11cf
Mayer, L., Fiacconi, D., Bonoli, S., et al. 2015, ApJ, 810, 51, doi: 10.1088/0004-637X/810/1/51
Mayer, L., Kazantzidis, S., Escala, A., & Callegari, S. 2010, Nature, 466, 1082, doi: 10.1038/nature09294
Mazzucchelli, C., Bañados, E., Venemans, B. P., et al. 2017, ApJ, 849, 91, doi: 10.3847/1538-4357/aa9185
McLeod, D. J., McLure, R. J., Dunlop, J. S., et al. 2021, MNRAS, 503, 4413, doi: 10.1093/mnras/stab731
Mihos, J. C., & Hernquist, L. 1996, ApJ, 464, 641, doi: 10.1086/177353
Moster, B. P., Naab, T., & White, S. D. M. 2018, MNRAS, 477, 1822, doi: 10.1093/mnras/sty655
Naidu, R. P., Matthee, J., Katz, H., et al. 2025, arXiv e-prints, arXiv:2503.16596, doi: 10.48550/arXiv.2503.16596
Nandal, D., & Loeb, A. 2025, arXiv e-prints, arXiv:2507.12618, doi: 10.48550/arXiv.2507.12618
Nandal, D., Zwick, L., Whalen, D. J., et al. 2024, A&A, 689, A351, doi: 10.1051/0004-6361/202449562
Natarajan, P. 2011, arXiv e-prints, arXiv:1105.4902. https://arxiv.org/abs/1105.4902
Natarajan, P., Pacucci, F., Ricarte, A., et al. 2024, ApJL, 960, L1, doi: 10.3847/2041-8213/ad0e76
O'Leary, J. A., Moster, B. P., Naab, T., & Somerville, R. S. 2021, MNRAS, 501, 3215, doi: 10.1093/mnras/staa3746
Pacucci, F., & Narayan, R. 2024, arXiv e-prints, arXiv:2407.15915, doi: 10.48550/arXiv.2407.15915
Pérez-González, P. G., Barro, G., Rieke, G. H., et al. 2024, ApJ, 968, 4, doi: 10.3847/1538-4357/ad38bb
Prieto, J., Jimenez, R., & Haiman, Z. 2013, MNRAS, 436, 2301, doi: 10.1093/mnras/stt1730
Prole, L. R., Regan, J. A., Glover, S. C. O., et al. 2024, A&A, 685, A31, doi: 10.1051/0004-6361/202348903
Regan, J. A., Downes, T. P., Volonteri, M., et al. 2019, MNRAS, 486, 3892, doi: 10.1093/mnras/stz1045
Regan, J. A., Johansson, P. H., & Wise, J. H. 2014, ApJ, 795, 137, doi: 10.1088/0004-637X/795/2/137
Regan, J. A., Wise, J. H., O'Shea, B. W., & Norman, M. L. 2020, MNRAS, 492, 3021, doi: 10.1093/mnras/staa035
Reines, A. E., & Volonteri, M. 2015, ApJ, 813, 82, doi: 10.1088/0004-637X/813/2/82
Reisswig, C., Ott, C. D., Abdikamalov, E., et al. 2013, PhRvL, 111, 151101, doi: 10.1103/PhysRevLett.111.151101
Rodriguez-Gomez, V., Genel, S., Vogelsberger, M., et al. 2015, MNRAS, 449, 49, doi: 10.1093/mnras/stv264
Rusakov, V., Watson, D., Nikopoulos, G. P., et al. 2025, arXiv e-prints, arXiv:2503.16595, doi: 10.48550/arXiv.2503.16595
Sacchi, A., & Bogdan, A. 2025, arXiv e-prints, arXiv:2505.09669, doi: 10.48550/arXiv.2505.09669
Saijo, M., & Hawke, I. 2009, PhRvD, 80, 064001, doi: 10.1103/PhysRevD.80.064001
Sassano, F., Capelo, P. R., Mayer, L., Schneider, R., & Valiante, R. 2022, arXiv e-prints, arXiv:2204.10330. https://arxiv.org/abs/2204.10330
Sassano, F., Schneider, R., Valiante, R., et al. 2021, MNRAS, 506, 613, doi: 10.1093/mnras/stab1737
Sawicki, M. 2002, AJ, 124, 3050, doi: 10.1086/344682
Schmidt, M. 1963, Nature, 197, 1040, doi: 10.1038/1971040a0
Schneider, R., Ferrara, A., Natarajan, P., & Omukai, K. 2002, ApJ, 571, 30, doi: 10.1086/339917
Schulze, A., Misawa, T., Zuo, W., & Wu, X.-B. 2018, ApJ, 853, 167, doi: 10.3847/1538-4357/aaa7f0
Setton, D. J., Greene, J. E., de Graaff, A., et al. 2024, arXiv e-prints, arXiv:2411.03424, doi: 10.48550/arXiv.2411.03424
Shakura, N. I., & Sunyaev, R. A. 1973, A&A, 24, 337
Shibata, M., Uchida, H., & Sekiguchi, Y.-i. 2016, ApJ, 818, 157, doi: 10.3847/0004-637X/818/2/157

Shlosman, I., Frank, J., & Begelman, M. C. 1989, Nature, 338, 45, doi: 10.1038/338045a0

Smith, B. D., Regan, J. A., Downes, T. P., et al. 2018, MNRAS, 480, 3762, doi: 10.1093/mnras/sty2103

Song, M., Finkelstein, S. L., Ashby, M. L. N., et al. 2016, ApJ, 825, 5, doi: 10.3847/0004-637X/825/1/5

Stahler, S. W., Shu, F. H., & Taam, R. E. 1980a, ApJ, 241, 637

—. 1980b, ApJ, 242, 226

—. 1981, ApJ, 248, 727

Stewart, K. R., Bullock, J. S., Wechsler, R. H., & Maller, A. H. 2009, ApJ, 702, 307, doi: 10.1088/0004-637X/702/1/307

Tacconi, L. J., Genzel, R., Saintonge, A., et al. 2018, ApJ, 853, 179, doi: 10.3847/1538-4357/aaa4b4

Tinker, J., Kravtsov, A. V., Klypin, A., et al. 2008, ApJ, 688, 709, doi: 10.1086/591439

Toomre, A. 1964, ApJ, 139, 1217, doi: 10.1086/147861

van Dokkum, P., Brammer, G., Baggen, J. F. W., et al. 2025, ApJL, 988, L6, doi: 10.3847/2041-8213/addcfe

Volonteri, M. 2012, Science, 337, 544, doi: 10.1126/science.1220843

Wang, B., de Graaff, A., Davies, R. L., et al. 2025, ApJ, 984, 121, doi: 10.3847/1538-4357/adc1ca

Wang, F., Yang, J., Fan, X., et al. 2021, ApJL, 907, L1, doi: 10.3847/2041-8213/abd8c6

Wiklind, T., Ferguson, H. C., Guo, Y., et al. 2019, ApJ, 878, 83, doi: 10.3847/1538-4357/ab1089

Williams, C. C., Alberts, S., Ji, Z., et al. 2024, ApJ, 968, 34, doi: 10.3847/1538-4357/ad3f17

Woods, T. E., Patrick, S., Elford, J. S., Whalen, D. J., & Heger, A. 2021, ApJ, 915, 110, doi: 10.3847/1538-4357/abfaf9

Woods, T. E., Agarwal, B., Bromm, V., et al. 2019, PASA, 36, e027, doi: 10.1017/pasa.2019.14

Yue, M., Eilers, A.-C., Ananna, T. T., et al. 2024, ApJL, 974, L26, doi: 10.3847/2041-8213/ad7eba

Zel'dovich, Y. B. 1964, Soviet Physics Doklady, 9, 195

Zhang, C., Wu, Q., Fan, X., et al. 2025, arXiv e-prints, arXiv:2505.12719, doi: 10.48550/arXiv.2505.12719

Zhang, S., Zhou, H., Shi, X., et al. 2018, AJ, 156, 4, doi: 10.3847/1538-3881/aac433

Zhou, H., Li, Z., Liao, K., et al. 2022a, ApJ, 928, 124, doi: 10.3847/1538-4357/ac510d

Zhou, H., Lian, Y., Li, Z., Cao, S., & Huang, Z. 2022b, MNRAS, doi: 10.1093/mnras/stac915

Zhu, Q., Li, Y., Li, Y., et al. 2020, arXiv e-prints, arXiv:2012.01458. https://arxiv.org/abs/2012.01458

Zwick, L., Mayer, L., Haemmerlé, L., & Klessen, R. S. 2023, MNRAS, 518, 2076, doi: 10.1093/mnras/stac3204